Contents lists available at SciOpen

Food Science and Human Wellness

journal homepage: https://www.sciopen.com/journal/2097-0765

China Food Publishing Co.

Prophylactic effects of sialylated glycopeptides from edible bird's nest on neuroinflammation in lipopolysaccharide-treated mice via the gut-brain axis

Xiangrong Cheng[a,b,*], Chenxi Zhang[a,b], Xiaoyi Zhao[a,b], Qiushi Li[a,b], Yu Song[a,c], Lan Zhang[d], Jiahui Ma[a,b], Yuyao Chen[a,b], Man Yuan[d], Dongliang Wang[a,d,*]

[a] *School of Food Science and Technology, Jiangnan University, Wuxi 214122, China*
[b] *State Key Laboratory of Food Science and Resources, Jiangnan University, Wuxi 214122, China*
[c] *Central Nervous System Product Research and Development Key Laboratory of Sichuan Province, Luzhou 646000, China*
[d] *Hebei Edible Bird's Nest Fresh Stew Technology Innovation Center, Langfang 065700, China*

ARTICLE INFO

Article history:
Received 30 January 2024
Received in revised form 3 March 2024
Accepted 24 April 2024

Keywords:
Edible bird's nest
Sialylated-glycopeptide
Neuroinflammation
Metabolomic
Gut microbiota

ABSTRACT

Edible bird's nest (EBN), abundant in sialic acid (SA) has been recognized as a natural substance beneficial to brain development and cognitive ability. In order to investigate active component of EBN, sialylated glycopeptides (SCP) were extracted from EBN by 60% ethanol after trypsin hydrolysis and its effects on central nervous system was evaluated in lipopolysaccharide (LPS)-induced neuroinflammation mice. EBN, SCP, and SA pretreatment and intervention reduced interleukin-1β (IL-1β), tumor necrosis factor-α (TNF-α), and interleukin-6 (IL-6) levels in hippocampus and cortex, meanwhile inhibited the activation of microglia, astrogliosis and neuron apoptosis, which were consistent with the learning and memory improvement and anti-depression effects in behavioral tests. The counts of leukocytes, neutrophils and monocytes, as well as IL-1β, TNF-α, and IL-6 levels in peripheral circulation were significantly reduced by SCP. Results of plasma metabolomics suggested SCP up-regulated energy metabolism, promoted the recovery of primary and secondary bile acid metabolism and indole metabolism, where microbiota may involve. 16S rDNA sequencing of colonic contents showed EBN, SCP and SA repaired dysbacteriosis in LPS-treated mice by significantly up-regulating the anti-inflammatory Muribaculaceae and inhibiting pro-inflammatory related *Desulfovibrio* and *Candidatus_Saccharimonas*. In addition, both EBN and SCP could significantly enrich *Aerococcus*, while SA could specifically enrich Prevotellaceae_UCG_001. The gut-brain axis was preliminarily established, and SCP may have the potential to be a functional factor for neuroprotection applied in EBN industry.

© 2025 Beijing Academy of Food Sciences. Publishing services by Tsinghua University Press.
This is an open access article under the CC BY-NC-ND license
(http://creativecommons.org/licenses/by-nc-nd/4.0/).

1. Introduction

WHO data have shown that the proportion of the elderly are on the rise worldwide. From 2020 to 2030, the population over 60 years old will increase from 1 billion to 1.4 billion, reaching over a sixth of the population. Aging is a major risk factor for many chronic diseases, among them, neurodegenerative diseases (NDs), such as Alzheimer's disease (AD), Parkinson's disease (PD), multiple sclerosis, accompanied by cognitive impairment, limb paralysis and other clinical manifestations, have put a heavy burden on patients and their families. Neuroinflammation is a pathological marker of NDs[1], as well as an important cause as more research confirmed[2]. It has been observed in neuroinflammatory response that microglia under specific conditions are over-activated and secrete a large number of pro-inflammatory cytokines such as tumor necrosis factor α (TNF-α),

* Corresponding authors at: School of Food Science and Technology, Jiangnan University, Wuxi 214122, China.
E-mail address: cheng-xiangrong@hotmail.com (X.R. Cheng); dongliang.wang@xxdun.com (D.L. Wang)
Peer review under responsibility of Beijing Academy of Food Sciences.

SciOpen Publishing services by Tsinghua University Press

http://doi.org/10.26599/FSHW.2024.9250289
2213-4530/©2025 Beijing Academy of Food Sciences. Publishing services by Tsinghua University Press. This is an open access article under the CC BY-NC-ND license (http://creativecommons.org/licenses/by-nc-nd/4.0/).

interleukin-6 (IL-6), IL-10, thus initiating the defense mechanism[3]. On the other hand, excessive pro-inflammatory cytokines activate the downstream pathways remarkably, which leads to the loss of nerve cells in the brain and the formation of amyloid β-protein (Aβ) causing brain damage in a long-term state, and cognitive impairment such as memory loss and depression[4-5]. As neuroinflammation induces and promotes pathological damage of the central nervous system, studies have focused on the intervention effects of nutrients on neuroinflammation and NDs[6].

Edible bird's nest (EBN) is saliva secreted by certain species of *Collocalia* swiftlets in Apodidae family that mainly distributed in Southeast Asian countries[7], which has a long history of consumption and medicine in Chinese population. Due to its abundant content of *N*-acetylneuraminic acid (approximately 10% of dry basis), the neuroprotective activity of EBN has been numerously reported[8-11], and its effect on the brain development and intelligence of offspring has been investigated as well[12-14]. Pharmacological studies have also shown that it has anti-inflammatory, and immunoregulatory effects in dextran sulfate sodium-induced ulcerative colitis[15] and 2,4-dinitrochlorobenzene-induced dermatitis[16].

The main component of EBN is protein, accounting on 50%–60% of dry weight, followed by carbohydrate[17]. Carbohydrates in EBN are in the form of oligosaccharides, which are composed of sialic acid (SA), galactose, *N*-acetyl glucose, *N*-acetyl galactose, mannose, and trace amounts of fucose and rhamnose mainly by *β*-glycosidic bonds[18-19]. SA is covalently bound to the non-reducing end of the sugar chain[20]. After *in vitro* digestion of stewed EBN gel, the undissolved SA reaches 56% and polysaccharide-bounded form is only 12% in total SA[21]. The Caco-2 cell model showed the absorption rate of EBN digestive products was quite limited[22]. Therefore, it's proposed that in the traditional Chinese way of EBN intake, EBN still has considerable indigestible components after passing through the digestive tract which will eventually reach the colon, directly contact with intestinal epithelial cells[23] or utilize by gut flora[19], where it is thus speculated that EBN play a beneficial role in human health. In this study, we suspect that sialylated-glycan is a prominent functional component in EBN and exert its bioactivities through gut microbiota regulation.

As a kind of biological macromolecule, the specific active components of EBN have always been a research hotspot. In this study, the trypsin-resistant glycopeptides of EBN were enriched to afford sialylated glycopeptides (SCP) that were highly unlikely to be absorbed by the host and even penetrated through the blood-brain barrier. The behaviors combined with biochemical index in hippocampus and serum were examined, multi-omics including plasma metabolomics and gut microbiome sequencing were conducted in lipopolysaccharide (LPS)-induced mice to evaluate the prophylactic effects and elucidated possible mechanism of SCP in improving cognitive impairment.

2. Materials and methods

2.1 Reagents and materials

EBN horn (originated from Malaysia, provided by Xiaoxiandun Biotechnology Co., Ltd., Beijing, China), SA (CS-02086, Kesitan Biotech Co., Ltd., Wuhan, China), trypsin (250 U/mg, Shanghai Yuanye Bio-Technology Co., Ltd., Shanghai, China), LPS (L2280, Sigma, USA), PBS tablets (Solarbio, Beijing, China), saline (Double-Crane Pharmaceutical Co., Ltd., China), glial fibrillary acidic protein (GFAP) antibody (A14673, Abclonal), ionized calcium binding adapter molecule-1 (IBA-1) antibody (Ab178846, Abcam), fluorescein 5-isothiocyanate (FITC) goat anti-rabbit antibodies (1111095-003, Jackson). Ethanol, $NaHSO_4$, *o*-phenylenediamine hydrochloride (OPD), glucose, phenol, sulfuric acid, methanol, acetonitrile, etc. were all purchased from Sinopharm Chemical Reagent Co., Ltd. (Shanghai, China). TNF-α (EHJ-45111m), IL-1β (EHJ-30026m), IL-6 (EHJ-30043m) commercial enzyme-linked immunosorbent assay (ELISA) kits were purchased from Xiamen Hui Jia Biotechnology Co. (Xiamen, China).

2.2 Preparation of SCP from EBN

Dry EBN horns were soaked with deionized water (1:49, *m*/*m*) at 4 ℃ for 12 h. Then swollen EBN was stewed in boiling water for 25 min to mimic traditional ways of intake in Chinses families. The cooked EBN gel was transferred to a grinder and crushed at high speed (5 s/time, 2–3 times) to get a uniform paste. Cooling at room temperature, homogenized EBN was added proper amount of water and then adjusted pH by adding 0.5 mol/L HCl solution to 8.0 (the optimum pH of trypsin is 7.8–8.5). The final ratio of trypsin in the reaction system was 10 000 U/g dry material, the material-liquid ratio was 1:29 (dry EBN horn:water, *m*/*m*), the optimum temperature ranged between 40–45 ℃ , and the oscillation frequency was set 200 r/min. Total hydrolysis process endured for 24 h. Reaction tubes were incubated at 95 ℃ for 10 min to inactivate enzymes. Enzymatic hydrolysis conditions were investigated and optimized previously in our labs.

Enzymatic hydrolysate then was added ethanol so that the volume fraction of ethanol in the final system reached 60%, mixed and rested for 10 min. Supernatant were obtained after centrifugation at 3 500 r/min for 20 min. Ethanol in supernatants were removed by rotary evaporator (R-205, Shenshen Biotech Co., Ltd., Shanghai, China) at 100 r/min and 40 ℃ in water bath. Steps above were repeated and finally get the concentrate. After being frozen at −80 ℃ for 12 h, the extracted SCP powder was obtained by a lyophilizer (SCIENTZ-10N, Scientz Biotech Co., Ltd., Ningbo, China).

2.3 Determination of SA, total carbohydrate content and molecular weight of SCP

The SA content was quantitatively determined by liquid chromatography (LC; LC-20AT, SHIMADZU, Japan). Firstly, 50 mg of grinded powder was added with 5 mL of 0.5 mol/L $NaHSO_4$ solution, then incubated under 80 ℃ water bath for 30 min to release SA. After cooling at room temperature, the mixture was added with 5 mL of OPD solution (10 g/L, dissolved with 0.25 mol/L $NaHSO_4$), and derived in 80 ℃ water bath for 40 min. The liquid was filtered by 0.22 μm filter membrane. LC working conditions: EF-C_{18} Bio column (Galaksil, China), temperature 30 ℃, acetonitrile-ultra-pure water (5:95, *V*/*V*), flow rate 1.0 mL/min, detection wavelength 230 nm, injection volume 20 μL.

Total carbohydrate content was analyzed by phenol-sulfuric acid method[24]. Certain amount of sample powder was added 1 mL of 5% phenol and 5 mL of sulfuric acid, vortexed and left to set for 20 min. The absorbance was read at 490 nm using a Microplate Reader 96 (EPOCH1, Bio Tek Instruments, Inc., USA). Glucose was used as a standard for making a concentration curve.

The molecular weight of SCP was determined by high performance gel filtration chromatography. Sample powder was

prepared into 10–15 mg/mL solution and analyzed after 0.22 μm filter membrane. Working conditions: Ultrahydrogel™ Liner column, refractive index detector, temperature 40 ℃, mobile phase: 0.1 mol/L sodium nitrate, flow rate 0.5 mL/min. Dextrans (T-5, T-10, T-150, T-300, T-2000) was used as standards.

2.4 Animals and treatments

Briefly, 40 male C57BL/6J mice (7-week-old, SPF grade) were purchased from Jiangsu GemPharmatech Co., Ltd. (Nanjing, China). All mice were raised in the barrier facility of Experimental Animal Center of Jiangnan University (SYXK(Su)2021-0056). The temperature and humidity were controlled at 20–26 ℃ and 40%–70% under pre-set dark-light cycle (12 h/12 h). During the adaptation period and the whole intervention cycle, the mice were fed with rodent chow pellet diets with access to water *ad libitum*. The experiment has been approved by the Experimental Animal Welfare and Ethics Committee of Jiangnan University, No. 20230415c0800705[145]. Mice were randomly divided into 5 groups (8 mice each), including the control (CON), the LPS (model), the EBN, the SCP and the SA group. After one week adaption, the CON and LPS group mice were given 0.2 mL of 0.9% saline by intragastric administration every day, and the intervention groups were given the same volume of EBN homogenate (200 mg/(kg·day)), extracted SCP and SA solution (the dose was calibrated according to the SA concentration in EBN) respectively for 7 consecutive weeks. Since the last week, the CON group received daily intraperitoneal injection of 0.9% saline, while the other groups were intraperitoneally injected LPS solution (500 μg/kg) for 7 consecutive days[25]. The flowchart is shown in Fig. 1. The behavioral test was carried out after 6 h of daily intraperitoneal injection. Finally, 24 h after all behavioral tests, the mice were sacrificed, tissue samples and colon contents were collected and frozen at –80 ℃ after quick freezing with liquid nitrogen.

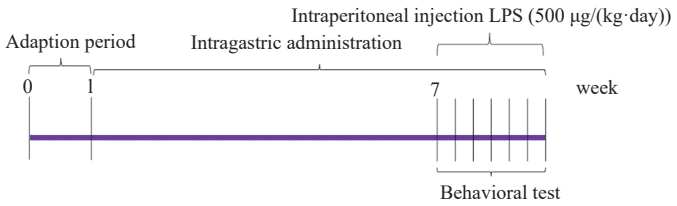

Fig. 1 Timeline of animal experiment.

2.5 Behavioral test

2.5.1 Morris water maze (MWM)

There was a round water tank (diameter 120 cm, height 50 cm) surrounded by an opaque cloth in the middle of the MWM device, where a platform (diameter 10 cm) was immersed into the 1 cm below the surface of the water. During the first 5 days, the mice were trained in directional navigation (hidden platform) test. Each mouse was placed into water from 4 different quadrants, with the task of finding the hidden platform within the time limit of 60 s. The escape latency and swimming track was recorded. If mice failed the task within 60 s, they were then guided to climb onto and stay on the platform for 15 s, so that the escape latency was recorded as 60 s.

On the 6th day, probe trail was conducted to evaluate memory consolidation. The platform was removed and the diagonal of the place where platform used to be was set as a new entry point (180° direction). The mice were allowed to swim freely for 60 s. The swimming path was monitored, the frequency across the front platform and the time spent in the target quadrant was recorded[26].

2.5.2 Y maze

The Y maze was composed of 3 arms of medical organic board (30 cm × 8 cm × 15 cm), and the angle between each arm was 120°. Each mouse was gently put into the starting arm, the movement in the 3 arms during 5 min was recorded, and the alternation percentage was calculated[27].

2.5.3 Open field test (OFT)

The device of OFT was a white open box (50 cm × 50 cm × 40 cm). A camera was installed directly above the box to record the movement track of the mice. Each mouse was gently placed on the side of the open box facing the wall, allowed to explore freely in 5 min. After each experiment, alcohol was sprayed, and stools and urine were removed. The analysis indexes included the time spent in the central area, immobility time, the total distance of movement, and the frequency of rearing[5].

2.6 Counts of leukocytes

Fresh blood was used to conduct cell count using an automatic hematology analyzer (BC-5000 Vet, Shenzhen Mindray Bio-Medical Electronics Co., Ltd., Shenzhen, China), including total white blood cells (WBCs), monocytes (Mon), neutrophils (Neu), eosinophils (Eos), basophils (Bas) and lymphocytes (Lym).

2.7 Determination of proinflammatory cytokines

The levels of TNF-α, IL-1β and IL-6 in serum and brain (hippocampus and cortex) homogenate of mice were determined by commercial ELISA kits, and the procedure was conducted according to the instructions. The absorbance was measured under 490 nm, and the cytokines were quantified according to the standard curve.

2.8 Nissl staining

Fresh brain was immersed into paraformaldehyde solution and was made into tissue sections after paraffin embedding, then dewaxed to water. Toluidine blue was added to stain for 2–5 min. After washing, 0.1% glacial acetic acid was added to differentiation, and then the reaction was stopped by distilled water before drying in the oven. Xylene was added and incubated for 10 min, and neutral gum was used to seal. The images were examined and collected under an optical microscope (NIKON ECLIPSE E100, Japan).

2.9 Immunofluorescence staining

Paraffin sections of brain were dewaxed to water, and then antigen repair was carried out with ethylenediaminetetraacetic acid

(EDTA) buffer (pH 8.0) in a microwave oven. After cooling at room temperature, the slides were placed in phosphate buffered saline (PBS) (pH 7.4), shaken and washed. Then 3% bovine serum albumin (BSA) was dripped to cover the tissue evenly, and the slide was incubated for 30 min. Then, slices were added with the first antibody dissolved in PBS (1:200 of glial fibrillary acidic protein (GFAP), 1:1 000 of ionized calcium binding adapter molecule (IBA-1), and put at 4 ℃ to incubate overnight. After decolorization and drying, the second antibody (1:400 dilution) was added and slides were incubated at room temperature overnight. The slides were then redyed with 4′,6-diamidino-2-phenylindole (DAPI) for 10 min before sealing. Images were captured using a slide scanner (3DHistech, Pannoramic DESK/MIDI/250/1000, Hungary), viewed by CaseViewer 2.5 software. Quantitative analysis was conducted using the average optical density with Image-Pro Plus 6.0 software (Media Cybemetics, USA).

2.10 Plasma metabolomics

The sample pretreatment of plasma and detection parameters based on liquid chromatography-tandem mass spectrometry (LC-MS/MS) was conducted following the previous procedure[28]. The chromatographic data file was imported into Compound Discoverer 3.3 software, simple screening, peak alignment and extraction was carried out. Then, the peak area was quantified, and the molecular formula was predicted and compared with mzCloud, mzVault, MassList database and self-built database (Shanghai Senschip Biotech Co., Ltd., Shanghai, China).

2.11 16S rDNA microbiota sequencing

High-throughput sequencing analysis of the gut microbiota in colonic contents was carried out according to Cheng et al.[29] with slight modification. Microbial DNA was extracted using the HiPure Stool DNA Kits (Magen, Guangzhou, China) according to manufacturer's protocols. The conserved V3-V4 region of bacterial rDNA was amplified with specific primers with barcode. The purified amplification products were mixed and the sequencing library was constructed in IlluminaPE250 (GeneDenovo Technology Co., Ltd., Guangzhou, China). USEARCH was selected to control the quality of the data, finally to obtain operational taxonomic units (OTUs) representative sequence and OTU abundance lists. Based on OTU and abundance tables, bioinformatics analysis was carried out.

2.12 Statistical analysis

The results were expressed as mean ± standard deviation (SD). GraphPad Prim 8.0 was used for statistical analysis and painting. For parametric test, one-way analysis of variance (ANOVA) was used to check the significance of difference among three groups and above, and multiple comparisons were made with Tukey model. Kruskal-Wallis test was applied in nonparametric test. $P < 0.05$ was set as threshold. Metabolomics data was filtered by using MetaboAnalyst 5.0 online platform (https://www.metaboanalyst.ca/), multivariate analysis and visualization was conducted by SIMCA13.0 software. Low abundance of OTU less than 0.5% of the total was filtered. A real-time and dynamic online Omicsmart platform (http://www.omicsmart.com) was used to filter, analyze and visualize the intestinal flora sequencing data.

3. Results

3.1 Characterization of EBN and its extracts

Key chemical composition and molecular weight of EBN and its extracts were preliminarily characterized. The total carbohydrate contents in EBN and SCP were (12.19 ± 0.38)% and (14.10 ± 0.20)%, and the SA contents were (10.94 ± 0.20)% and (12.11 ± 0.67)% respectively. The proportion of SA was similar, but the existing form differed. As shown in Table 1, extracted SCP included three major fractions, whose number average molecular weight (M_n) ranged from 385 to 6 444 Da, whereas the main component of EBN was glycoprotein with the molecular weight over 10 kDa[30].

Table 1
Average molecular weight of SCP.

Fraction	Area (%)	M_n (Da)	M_w (Da)	M_p (Da)
1	63.87	6 444	14 044	5 930
2	14.87	1 239	1 329	1 186
3	21.26	385	457	571

Note: M_w, weight average molecular weight; M_p, peak molecular weight.

3.2 SCP alleviated learning and memory impairment and depression-like behaviors

The body weight (BW) of groups mice shifted during the 7-day behavioral test. As Fig. 2A showed, the BW of CON group mice remained stable and increased slightly during 7 days. On the contrary, the BW of LPS group mice continuously and significantly declined till to the 3rd day ($F(6,44) = 3.479$, $P < 0.01$) and then increased slowly in the next 4 days to the level of no significance with the 1st day. BW changes of mice in EBN, SCP and SA groups were similar to that of LPS group.

Behavioral experiments were widely used to test the cognitive ability and mental state of mammalian rodents. During the training period of MWM test, the latency of mice in CON group shortened day by day. On the contrary, the time taken to reach the platform in LPS group was significantly higher than that in CON group on the 2nd day ($F(4, 32) = 3.939$, $P < 0.01$), and it lasted until the 5th day ($F(4, 25) = 3.390$, $P < 0.001$), suggesting that the spatial memory and learning abilities of LPS mice were impaired. Compared with LPS group, the latency of mice in EBN, SCP and SA groups shortened on the days 2 to 5, and that of SCP group on the days 3 to 5 was significantly shorter ($P < 0.05$), suggesting the improvement of learning and memory ability (Fig. 2B). After removing the platform on the 6th day, the mice were allowed to explore 5 min freely in the water maze (probe trial). It was found that the time of LPS mice spent in the target quadrant was less than that of the CON group, and the frequency of passing through the target quadrant significantly decreased ($F(4, 33) = 7.474$, $P < 0.001$), suggesting that the long-term memory retention ability of LPS mice declined (Figs. 2C and D). However, the time and passing frequency in the target quadrant of EBN, SCP and SA groups increased, suggesting that EBN and its potential active components contributed to relieving the decline of long-term memory.

Y maze was a classic experiment to test the short-term working memory ability of mice. The spontaneous alternation percentage in LPS mice significantly decreased compared with CON mice ($F(4, 29) = 3.916$, $P < 0.05$), while that in EBN, SCP and SA mice was significantly

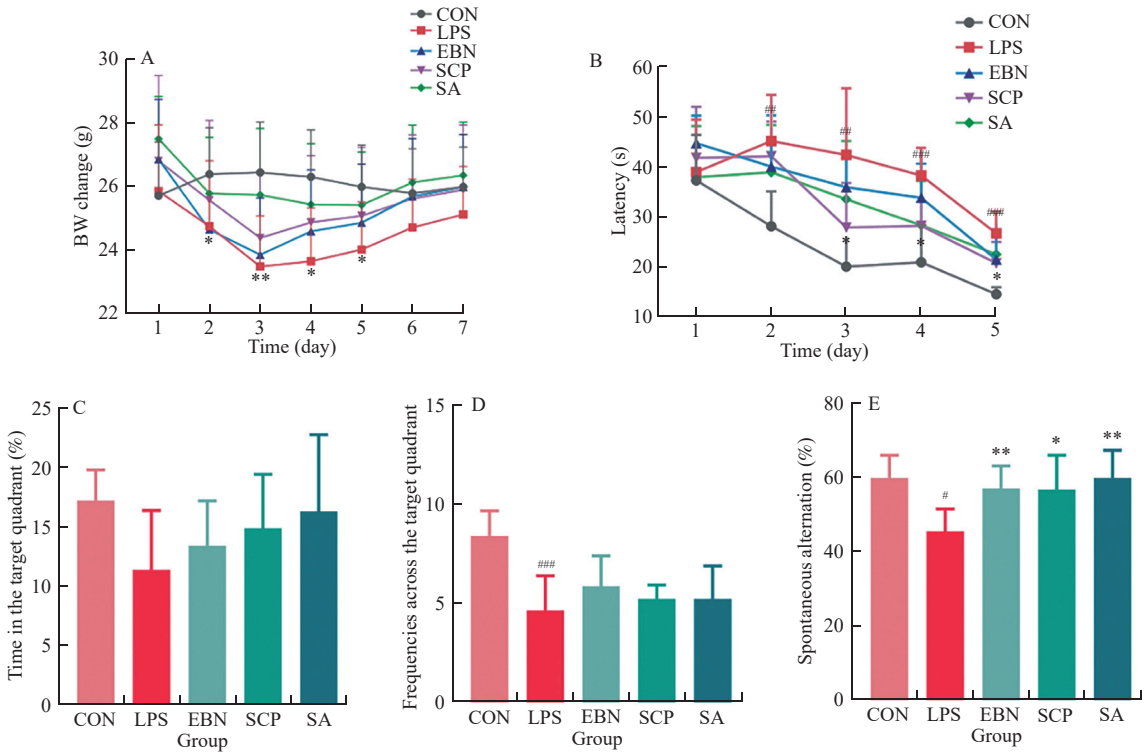

Fig. 2 Effects of EBN, SCP and SA on BW, learning and memory ability in LPS-treated mice. (A) Changes in BW of mice during 7 days of daily intraperitoneal injection of LPS. $n = 8$. $^{*}P < 0.05$, $^{**}P < 0.01$ *vs*. Day 1. (B) Latency of different groups of mice during training period. (C-D) Long-term memory ability of mice in probe trail. (E) Working memory of mice in Y maze. $n = 8$. $^{\#}P < 0.05$, $^{\#\#}P < 0.01$, $^{\#\#\#}P < 0.001$ *vs*. CON group, $^{*}P < 0.05$, $^{**}P < 0.01$ *vs*. LPS group.

increased compared with LPS mice ($P < 0.05$, 0.01), showing that EBN and its potential active products could alleviate the decline of short-term memory induced by LPS (Fig. 2E). In summary, EBN, SCP and SA could alleviate LPS-induced learning and memory impairment and improve memory performance.

The movement, self-care and other behaviors of mice in the OFT could be used as indicators to judge whether there was a tendency to get anxious and depressed in mice. Compared with CON group, the time in central zone ($F(4, 31) = 3.276$, $P < 0.01$), the total moving distance, and the frequency of rearing of LPS mice reduced ($F(4, 29) = 3.629$, $P < 0.05$), while the immobility time increased ($F(4, 27) = 2.941$, $P < 0.05$). These results indicated that LPS mice exhibited depression-like behavior. Compared with LPS group, EBN and SA intervention increased the time in the central area, increased the moving distance, and shortened the immobility time. Interestingly, SCP group mice were shown more time staying in central zone ($P < 0.01$), higher frequency rearing ($P < 0.05$), and less time being still ($P < 0.05$). Therefore, it was found that EBN, SCP and SA was able to alleviate LPS-induced depression-like morbidity (Fig. 3).

3.3 SCP alleviated neuroinflammation and protected neurons

Intraperitoneal injection of LPS could cause strong and instant expression of IL-1β, IL-6 and TNF-α in various brain regions of mice. As Fig. 4A and Table S1 showed, compared with CON group the expression of IL-1β, TNF-α and IL-6 in hippocampus rose and those levels in cortex increased significantly ($F(4, 15) = 3.676$, $F(4, 13) = 3.479$, $F(4, 13) = 3.87$; $P < 0.05$), suggesting neuroinflammation in the LPS-treated mice. Under the intervention of EBN, SCP and SA, the expression of IL-6 in cortex declined significantly ($P < 0.05$), and in SA

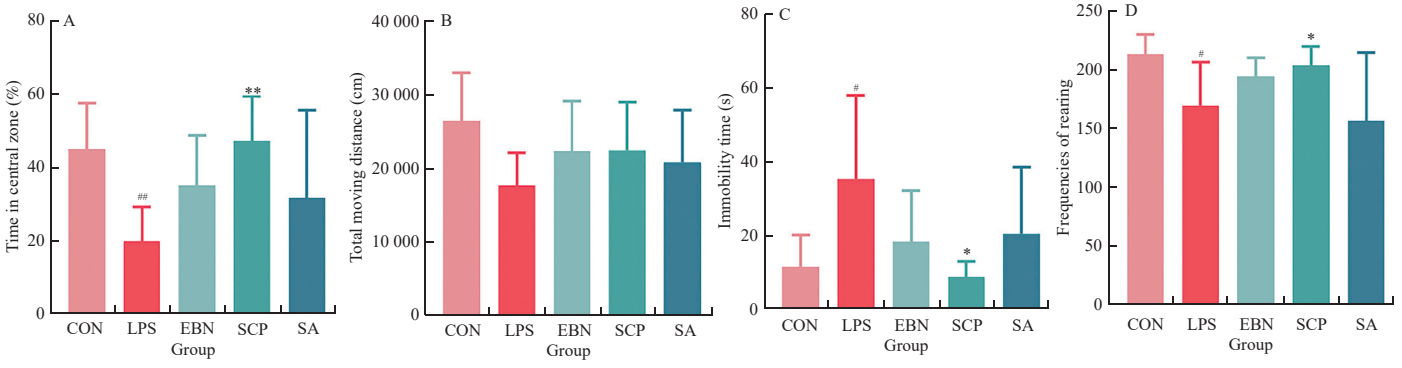

Fig. 3 Effects of EBN, SCP and SA on depression-like behavior in LPS-treated mice. $n = 8$. $^{\#}P < 0.05$, $^{\#\#}P < 0.01$ *vs*. CON group, $^{*}P < 0.05$, $^{**}P < 0.01$ *vs*. LPS group.

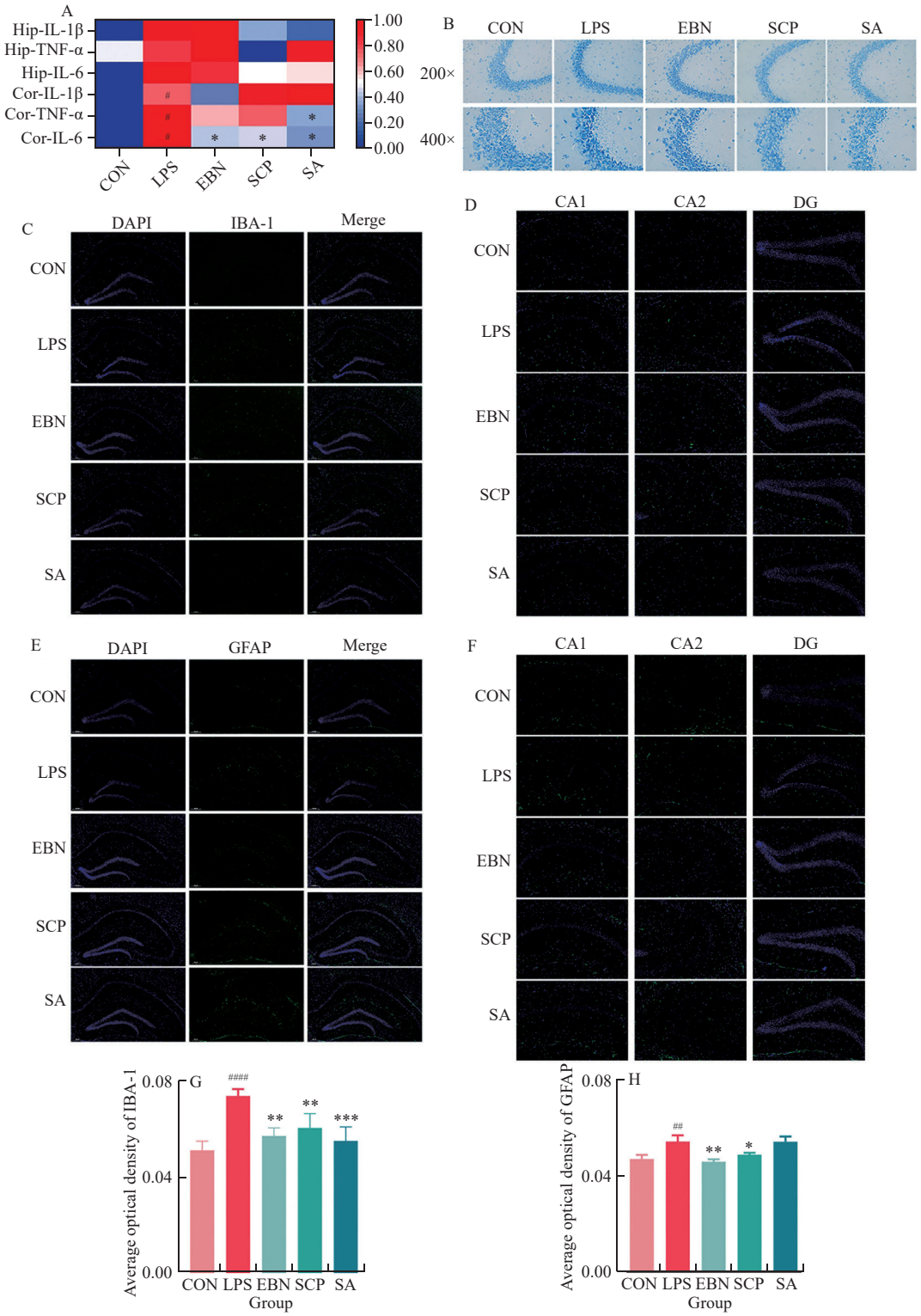

Fig. 4 Effects of EBN, SCP and SA on neuroinflammation. (A) Heatmap of pro-inflammatory cytokines in hippocampus (Hip) and cortex (Cor). $n = 4$. $^{\#}P < 0.05$ *vs*. CON, $^{*}P < 0.05$ *vs*. LPS. (B) Morphology and structure of neurons in CA2 region of hippocampus. $n = 3$. Panoramic images of immunostaining of (C) IBA-1 and (E) GFAP proteins in the hippocampus was performed with specific primary antibodies. Representative images of CA1, CA2 and dentate gyrus (DG) region in hippocampus for (D) IBA-1 and (F) GFAP immunostaining (20×). (G-H) Quantitative statistical analyses were conducted with average optical density. $^{\#\#}P < 0.01$, $^{\#\#\#\#}P < 0.000\ 1$ *vs*. CON group, $^{*}P < 0.05$, $^{**}P < 0.01$, $^{***}P < 0.001$ *vs*. LPS group.

group, TNF-α level showed significant decrease ($P < 0.05$), but the expression of IL-1β was no significance under the intervention. In addition, SCP decreased the levels of these inflammatory cytokines in the hippocampus. It is suggested that EBN, SCP and SA alleviated the increase of inflammatory cytokines in the brain induced by LPS and exerted the regulatory activity of neuroinflammation.

Hippocampus played an important role in integrating information from short-term memory to long-term memory, spatial memory and

emotional regulation. Therefore, activation of cells responding to neuroinflammation and structure of neurons in the hippocampus was detected. IBA-1 was a specific intracellular protein of microglia, which often used as a specific marker. GFAP was used as a biomarker of astrocyte proliferation (or astrogliosis) in central nervous system injury. Immunofluorescence staining showed that the activation of microglia indicated by IBA-1 staining was significantly enhanced ($F(4, 19) = 11.60$, $P < 0.000\ 1$) and the astrogliosis indicated by GFAP staining increased ($F(4, 10) = 14.84$, $P < 0.01$) as well in LPS mice. Nevertheless, the activation of microglia was significantly alleviated by EBN, SCP and SA ($P < 0.01$, 0.001), meanwhile, astrogliosis was inhibited by EBN and SCP ($P < 0.05$) in hippocampus (Figs. 4C-H). Consequently, EBN, SCP and SA alleviated the activation of glial cells in LPS-treated neuroinflammation.

Results of Nissl staining revealed the morphological changes of neurons in hippocampal CA2 region. As shown in Fig. 4B, the number of neurons in CON group was abundant, and the cells possessed complete structural outline and clear nucleolus. While in the LPS group, the number of neurons decreased significantly, and cell lysis appeared in the marginal layer accompanied by diffusing cell fragments, and the remaining cells contracted irregularly with dense nucleoli. Compared with LPS group, the number of neurons in EBN group increased, there were still some apoptotic cells but fragments decreased. A greater number of intact cells appeared in SCP group. While in SA group, neurons were loosely arranged with hollow and cell fragments, and the structural integrity decreased. Thus, EBN, SCP and SA could prevent neuronal death and structural destruction induced by LPS in different degrees.

3.4 SCP decreased leukocytes and pro-inflammatory cytokines in peripheral circulation

Leukocytes and pro-inflammatory cytokines in peripheral circulation were measured to evaluate the systemic inflammation. After LPS-exposure for 7 days, total WBC ($F(4, 18) = 4.955$, $P < 0.05$), Neu ($F(4, 17) = 5.766$, $P < 0.001$), Mon ($F(4, 15) = 7.405$, $P < 0.001$), Eos ($F(4, 16) = 4.695$, $P < 0.01$) and Bas (Kruskal-Wallis, $P < 0.01$) increased significantly (Figs. 5A-E). There was no difference in the number of Lym ($F(4, 20) = 2.076$, $P > 0.05$, Fig. 5F). Compared with LPS group, total WBC in EBN, SCP and SA groups all significantly reduced ($P < 0.05$). There was also a reduction in Neu, Mon, Eos and Bas number in EBN mice, while SCP and SA intervention decreased Neu ($P < 0.05$) and Mon ($P < 0.05$) significantly.

Levels of IL-1β, TNF-α and IL-6 in serum were further determined (Figs. 5G-I). Compared with CON group, serological IL-1β, TNF-α ($F(4, 15) = 5.412$, $P < 0.01$) and IL-6 ($F(4, 21) = 4.311$, $P < 0.05$) in LPS mice increased. Compared with LPS group, the expression of IL-1β, TNF-α and IL-6 in mice treated with EBN, SCP and SA decreased. Among them, EBN decreased IL-1β ($F(4, 15) = 4.135$, $P < 0.05$) and TNF-α ($P < 0.05$) significantly, while SCP relieved IL-1β and IL-6 significantly ($P < 0.05$).

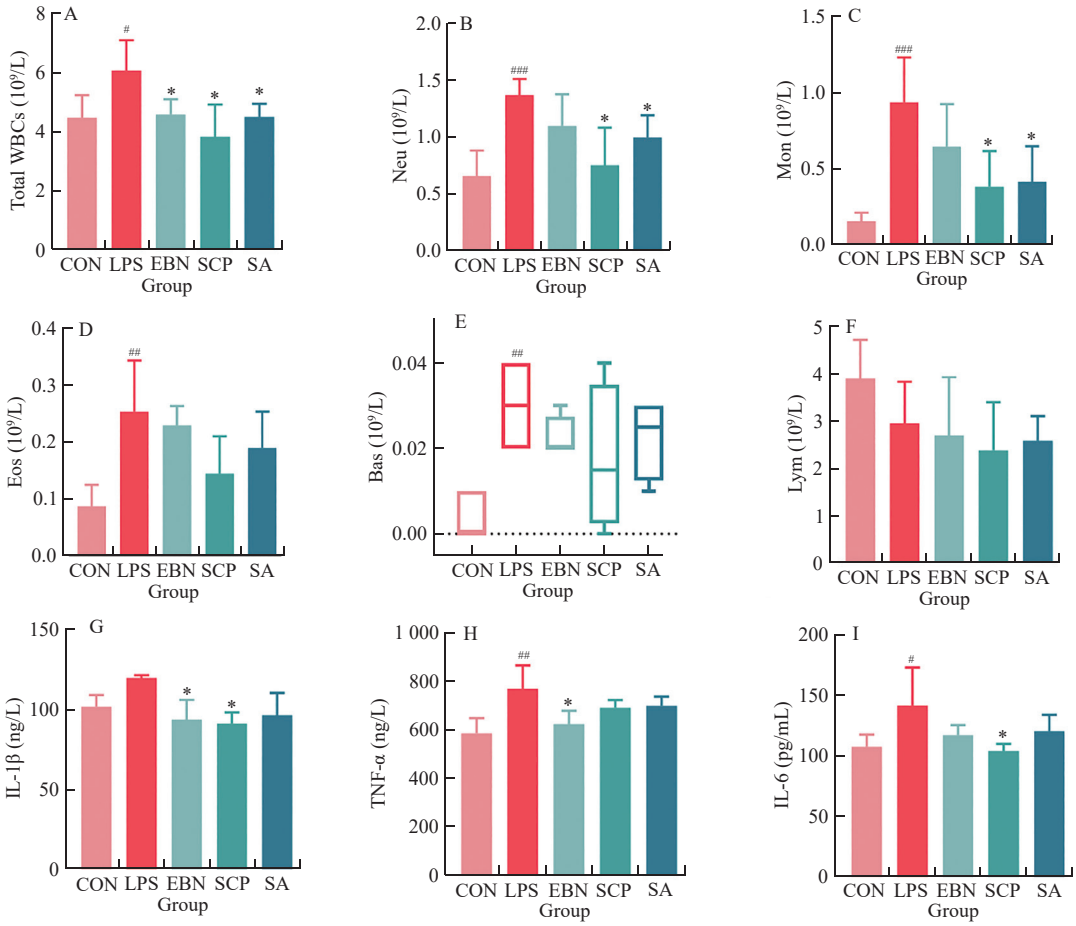

Fig. 5 Regulatory effects of EBN, SCP and SA on leukocytes and pro-inflammation cytokines in peripheral circulation. (A-F) Counting of total and subtype WBCs, $n = 5$. (G-I) Levels of IL-1β, TNF-α and IL-6 in serum. $n = 4$–5. $^{\#}P < 0.05$, $^{\#\#}P < 0.01$ *vs*. CON group, $^{*}P < 0.05$, $^{**}P < 0.01$ *vs*. LPS group.

3.5 SCP regulated plasma metabolites through pathways of tricarboxylic acid (TCA) cycle, primary bile acid biosynthesis, and indole metabolism

Based on the LC-MS/MS platform, the high-throughput data of mouse plasma metabolites was obtained. There were 2 475 (negative ion mode) and 3 781 (positive ion mode) chromatographic features obtained after MS signal extraction, quality control (QC) and interquartile difference (IQR) filtering. Multivariate statistical models were then established, including principal component analysis (PCA) and orthogonal partial least square-discriminant analysis (OPLS-DA).

PCA was an unsupervised classification model, used to observe the natural distribution trend of the metabolic profiles. First of all, Hotelling's T^2 (Figs. 6B and F) showed all the sample points lied below 99% confidence interval, indicating there was no outliners needed to be eliminated. Under the UV scaling in PCA mode, the QC samples got close indicating the analyzed instrument and methods were stable and reliable, and sample points in each group were concentrated as well (Figs. 6A and E). From the view of PC1, the CON group was obviously separated from the other four groups, suggesting that the metabolism of LPS-induced neuroinflammation mice had changed remarkably. On the PC2, it was found that EBN, SCP and SA were far away from the LPS group, suggesting that the metabolic profile of mice had been intervened. Among them, SCP stayed closest to CON group, implying a better callback effect.

OPLS-DA model was set based on the pre-classified data, thus permutation test was used to verify the reliability of the supervised model (Figs. 6C, D, G and H). In the OPLS-DA diagram, separation of experimental groups in two-dimensional space was quite obvious. All samples displayed a similar distribution to that in PCA diagram. LPS treatment made a significantly different metabolic profile from the CON group, which was consistent with the changes in behavioral, physiological and biochemical indicators investigated. EBN and SCP groups were clustered closer, while SA displayed an obvious separation trend from EBN and SCP. That indicated EBN and SCP exerted similar regulatory effects on plasma metabolites in mice with neuroinflammation, while the metabolic changes caused by SA owned particularity.

$P < 0.05$ and VIP > 1.0 was set as the threshold, and 39 differential metabolites were identified in the negative ion mode and meanwhile 15 in the positive ion mode (Fig. 7A). Compared with CON group, it was found that oxoglutaric acid, succinic acid, fumaric acid and malic acid in plasma decreased significantly in LPS mice. These substances were involved in TCA circulation, metabolism of alanine, aspartic acid and glutamic acid and arginine biosynthesis, suggesting abnormal metabolism of energy and related amino acids. Cholic acid and 3-dehydrocholic acid decreased significantly, while taurocholic acid,

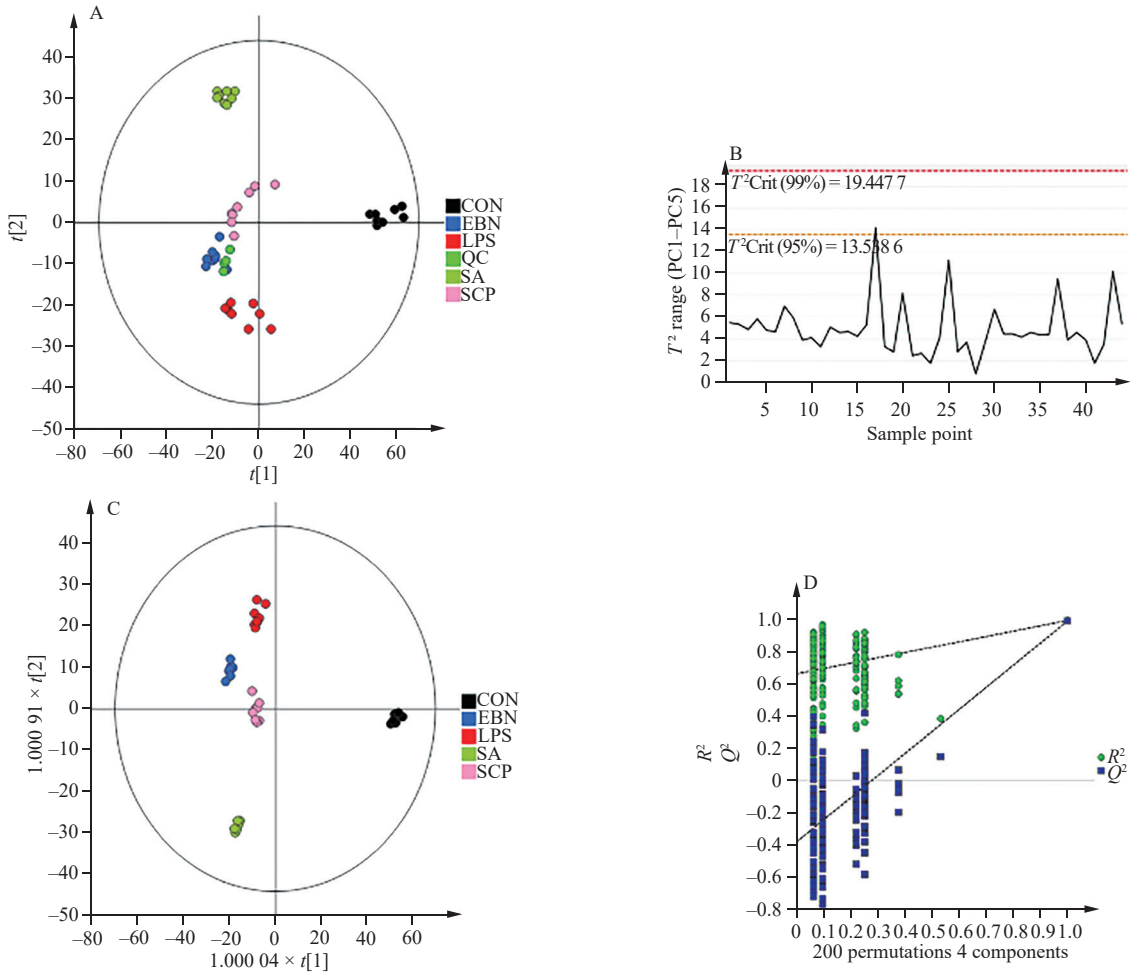

Fig. 6 Effects of EBN, SCP and SA on metabolic profiles in plasma of LPS-treated mice. $n = 8$. (A, E) PCA diagram. (B, F) Hotelling's T^2 showed none of outliners in both iron mode. (C, G) OPLS-DA diagram. (D, H) Permutation figure indicated models passed the test without over-fitting. (A-D) Negative iron mode; (E-F) positive iron mode.

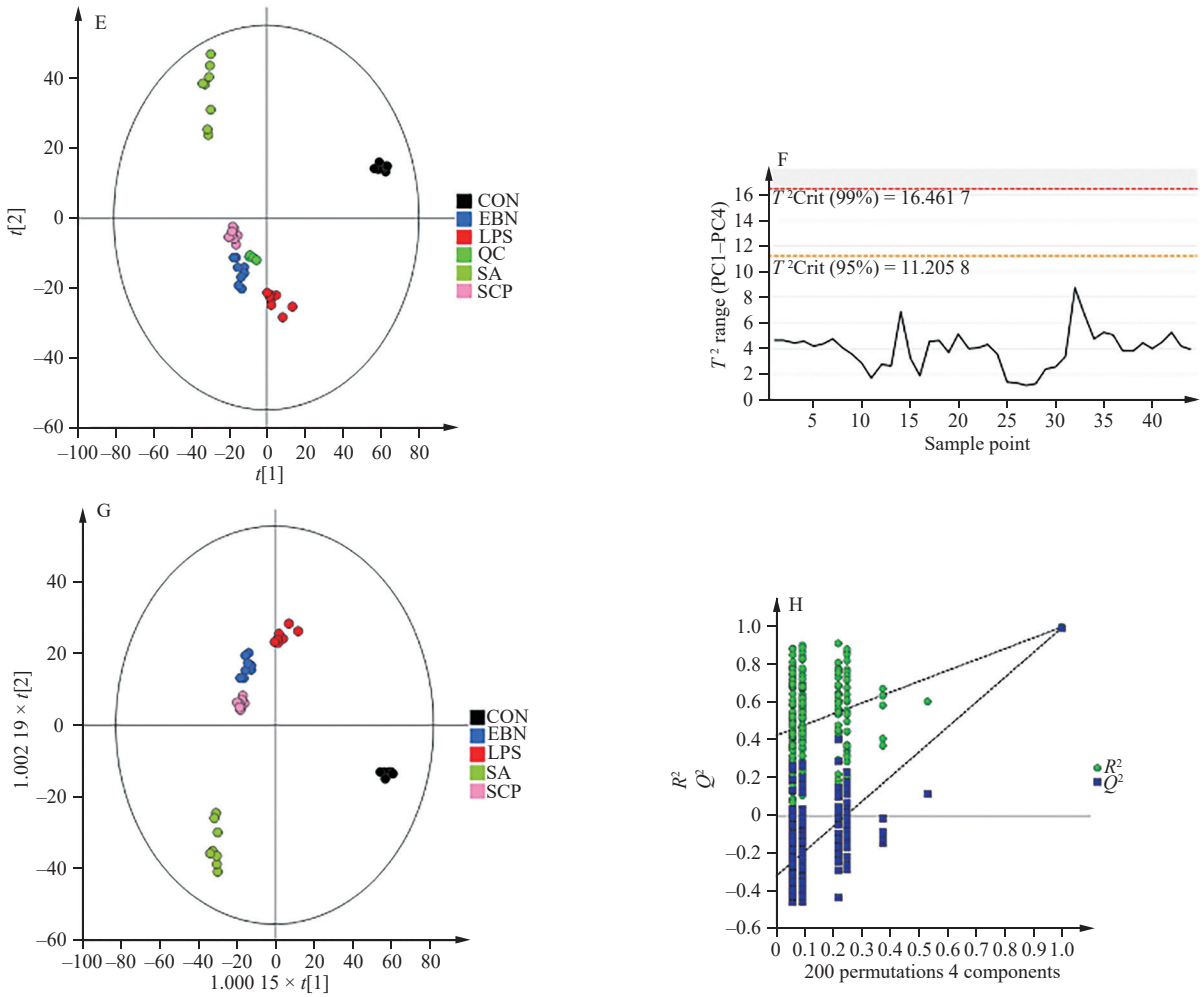

Fig. 6 (*Continued*)

taurochenodeoxycholic acid and deoxycholic acid increased significantly, suggesting a significant change in the composition of bile acid pool (Figs. 7A, 8A-D). Among the substances related to pyrimidine and purine metabolism, it was found that 5-thymidylic acid decreased significantly, orotic acid increased significantly, xanthosine and hypoxanthine decreased significantly. In addition, *L*-tryptophan and indole decreased significantly, while the concentrations of indole-3-propionic acid (IPA) and 3-indoleacrylic acid increased (Figs. 8E-H). Besides, fatty acids and derivatives involved in energy metabolism and functioning as signal molecule had changed, for example, *L*-acetylcarnitine, *L*-palmitoylcarnitine, oleoylcarnitine, arachidonic carnitine, and 11,12-epoxyeicosatrienoic acid, 18*R*-hydroxy-5*Z*,8*Z*,11*Z*,14*Z*,16*E*-eicosapentaenoic acid (18*R*-HEPE) and FA 18:5+2O decreased significantly, while docosatrienoic acid and 2-arachidonicglycerol increased significantly. Glycine derivatives such as acetylglycine, hexanoylglycine and 3-methylcrotonylglycine reduced significantly. The results above suggested there occurred metabolic disorders in LPS mice, and EBN, SCP and SA played a regulatory role in different ways.

Kyoto Encyclopedia of Genes and Genomes (KEGG) and Relational Database of Metabolomic Pathways (RaMP) were used to find out differential metabolic pathways (Table 2). Based on $P < 0.05$ and impact value > 0, there were TCA cycle, metabolism of alanine, aspartate and glutamate and biosynthesis of primary bile acid enriched in LPS group, and additional indole metabolism in the gut-liver was found in the RaMP library. According to KEGG database, the pathway enriched in EBN group was primary bile acid biosynthesis, the pathways enriched in SCP group were primary bile acid biosynthesis, TCA cycle, alanine, aspartate and glutamate metabolism and pyrimidine metabolism. The pathway enriched in SA group was primary bile acid biosynthesis. Accordingly, there were more coincident pathways between SCP and LPS, suggesting that it might play a better role in regulating the metabolic pathway (Figs. 7B and C).

3.6 *SCP regulated dysbacteriosis in LPS-treated mice*

Colon microbiota was analyzed by 16S rDNA sequence. First of all, the dilution curve showed the sequencing was sufficient and ensured data reliable (Fig. 9A). Secondly, the overall ecological structure of gut flora was observed. α-Diversity referred to the diversity in a specific ecosystem, and observed species (Sobs), Chao1, ACE, Pielou's evenness, Shannon, and Simpson indexes were commonly used. As shown in Table 3, Sobs, Chao1 and ACE indexes in CON and LPS group was higher than that in SCP, SA and EBN groups, but without statistical difference ($P > 0.05$). Shannon and Simpson indexes were concerned about both richness and evenness.

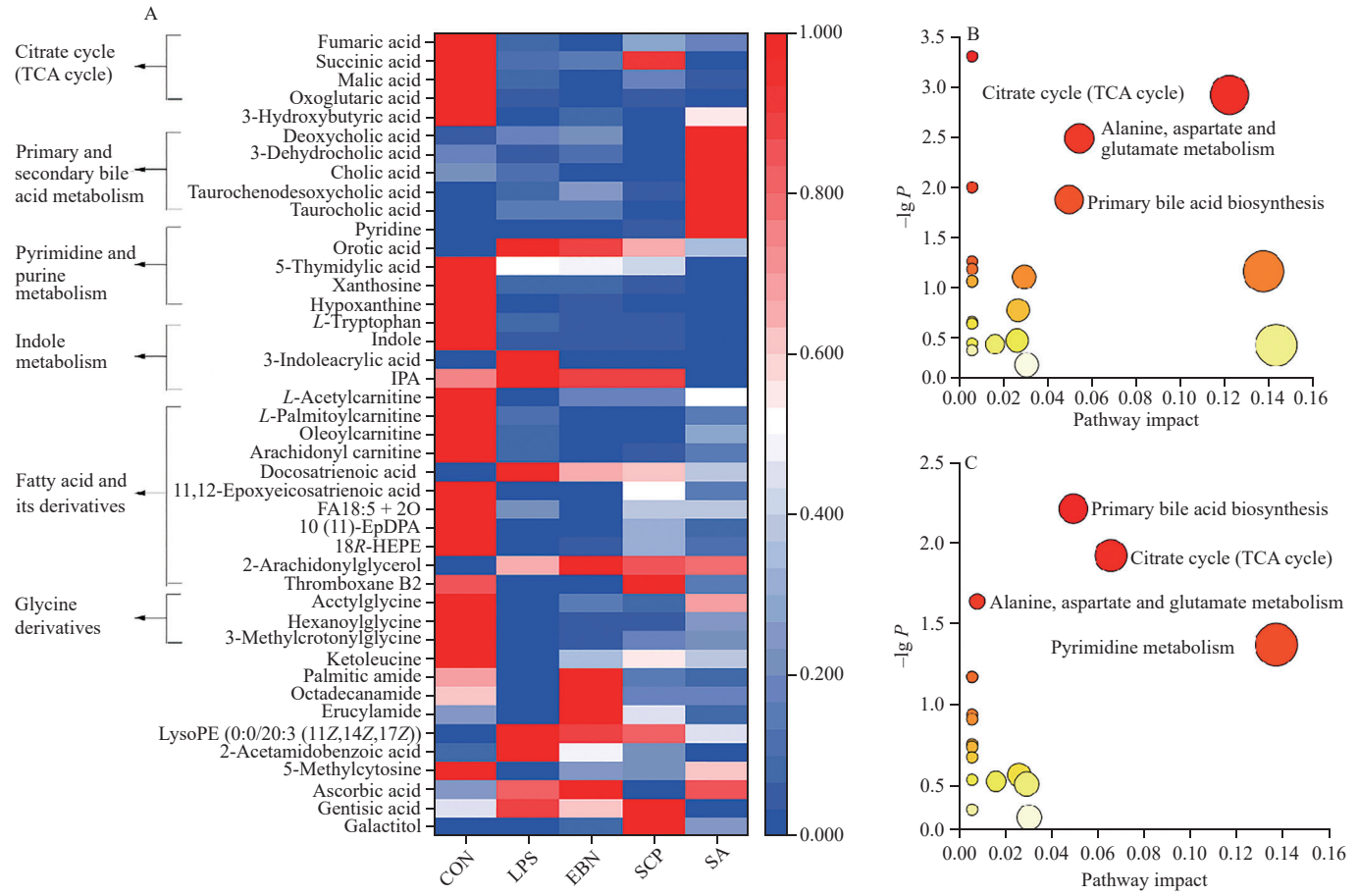

Fig. 7 Differential metabolites and pathways in different groups of mice. $n = 8$. (A) Heatmaps of differential metabolites between CON, LPS, EBN. SCP and SA groups (negative ion mode). Differential metabolic pathways of (B) LPS and (C) SCP searched in KEGG database.

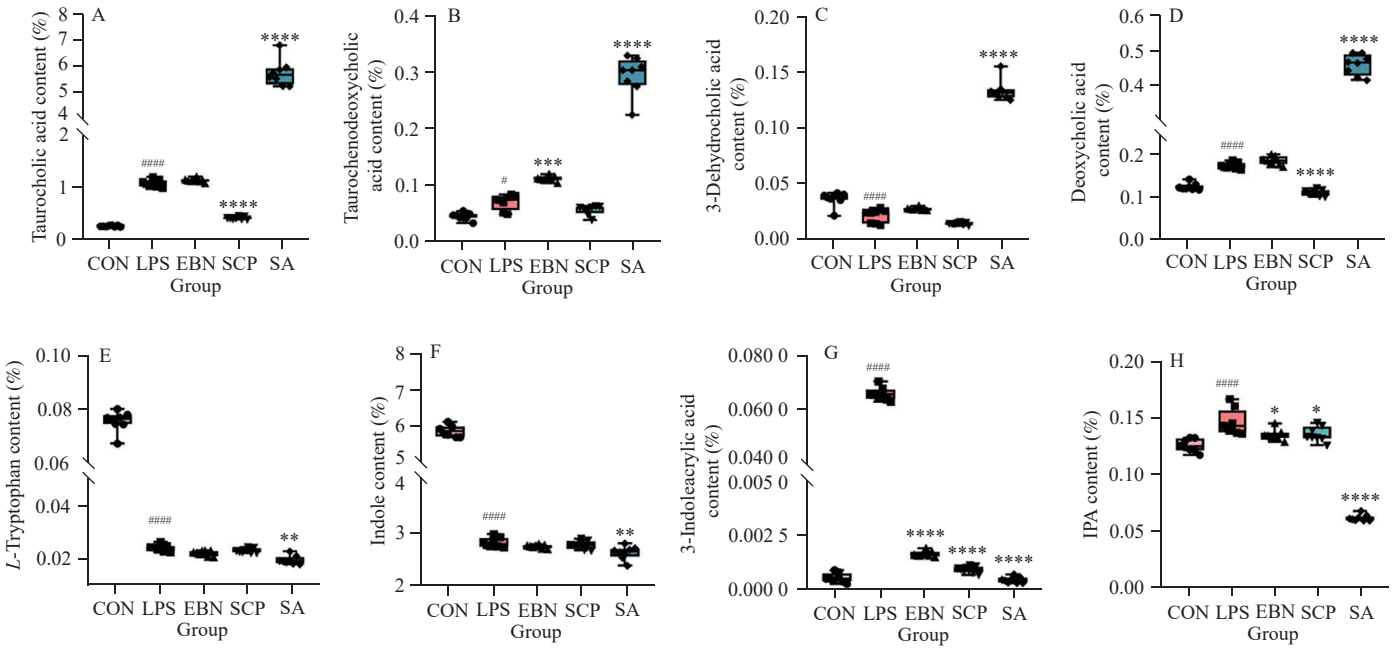

Fig. 8 Representative substances in (A-D) primary and secondary bile acid metabolism and (E-H) indole metabolism. $n = 8$. $^{\#}P < 0.05$, $^{\#\#\#\#}P < 0.000\ 1$ *vs*. CON group, $^{*}P < 0.05$, $^{**}P < 0.01$, $^{***}P < 0.001$, $^{****}P < 0.000\ 1$ *vs*. LPS group.

Table 2
Differential metabolic pathways searched in KEGG and RaMP database.

Group	Pathway	*P* value	FDR	Impact
LPS	TCA cycle	0.001 21	0.050 9	0.121
	Alanine, aspartate and glutamate metabolism	0.003 29	0.009 21	0.050 5
	Primary bile acid biosynthesis	0.013 4	0.226	0.045 7
EBN	Gut-liver indole metabolism	0.000 002 13	0.001 01	/
	Primary bile acid biosynthesis	0.028 7	0.269	0.022 9
SCP	Primary bile acid biosynthesis	0.006 16	0.503	0.045 7
	TCA cycle	0.012 0	0.503	0.062 5
	Alanine, aspartate and glutamate metabolism	0.022 9	0.642	0.002 40
	Pyrimidine metabolism	0.042 6	0.894	0.137
SA	Primary bile acid biosynthesis	0.011 3	0.748	0.045 7

Note: FDR, false discovery rate; smaller value means larger possibility.

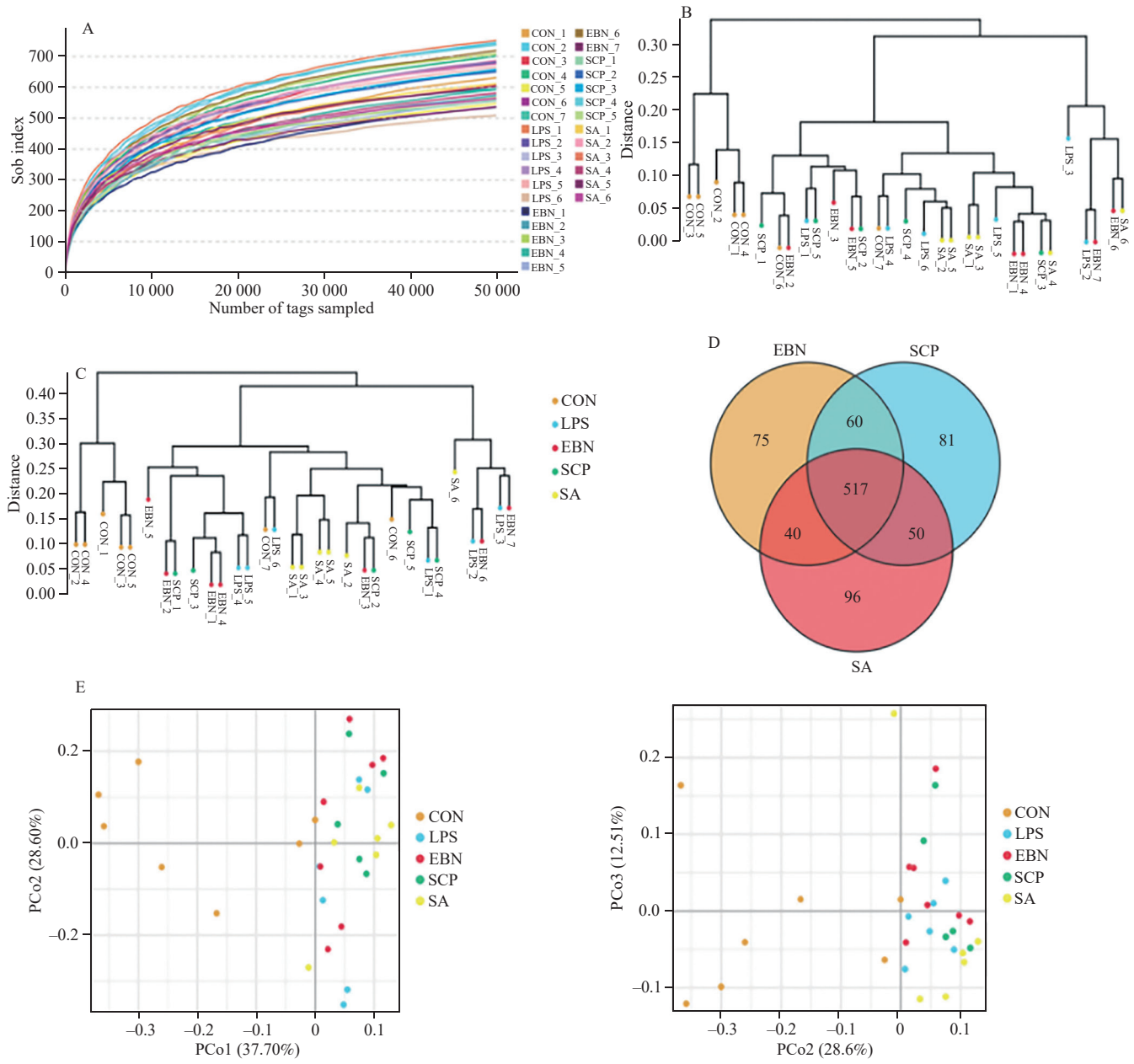

Fig. 9 Diversity and composition of gut microbiota. n = 5–7. (A) Dilution curves. Cluster trees at (B) phylum and (C) family level. (D) Venne diagram of EBN, SCP and SA groups at OTU level. (E) PCoA of the community structure at family level evaluated by Bray-Curtis distances.

There was no significant difference in Shannon index. Whereas, the Simpson index of LPS group increased significantly compared with that of CON group ($P < 0.05$), indicating its microbiota structure become more abundant. Pielou's evenness of LPS group significantly higher than that in CON group ($P < 0.05$). More uniform species distribution in LPS group explained the increase of Shannon and Simpson indexes.

β-Diversity expressed by distance values was used to measure similarity between communities, visualized by cluster tree and principal coordinates analysis (PCoA). Cluster analysis showed that samples in LPS mice were scattered at phylum and family level, suggesting there was great heterogeneity in flora structure among mice with neuroinflammation. In contrast, healthy CON mice were clustered closely, and the EBN and SCP samples got closer to the CON group as a whole (Figs. 9B and C). The PCoA at the family level was drawn based on Bray-Curtis distance, and the proportion of PCo1, PCo2 and PCo3 was 37.70%, 28.60% and 12.51%, respectively (Fig. 9E). The CON group was significantly separated from other samples, and the rest of the intervention group showed a separating trend from LPS group. The P value and R^2 of scatter plot was 0.001 and 0.331 (Adonis test), which showed that there were statistical differences among microbial communities.

Gut microflora composition was displayed in stacking map at phylum, family and genus level (Fig. 10). At the phylum level, the relative abundance of Bacteroidota, Firmicutes and Verrucomicrobia in CON group was 36.43%, 32.13%, and 21.17% respectively, making up 89.73% of the total. Desulfobacterota and Patescibacteria accounted for 5.79%, 2.56% and the rest was less than 1%. Compared with CON group, Firmicutes and Bacteroidota ratio (F/B) increased ($P < 0.05$), Verrucomicrobia abundance decreased significantly ($P < 0.000\ 1$), but the abundance of Desulfobacterota ($P > 0.05$), Patescibacteria ($P < 0.001$) and Deferribacterium ($P < 0.001$) in colon of LPS group increased (Figs. 11A–E). An increase of bacteria related to abnormal metabolism combined with a descend in normal and beneficial bacteria suggested the intestinal microflora disorder. Compared with LPS group, Verrucomicrobia in EBN increased, while the F/B ($P < 0.05$), the abundance of Desulfobacterota ($P > 0.05$), Patescibacteria ($P < 0.001$) and Deferribacterium ($P < 0.001$) decreased. The major composition of SCP group was similar to that of EBN group, but the abundance of Verrucomicrobia was much lower than that of EBN. The top three bacteria in SA group were also Bacteroidota, Firmicutes and Desulfobacterota but the proportion of Desulfobacterota was higher than that of EBN and SCP groups, with a lower abundance of Verrucomicrobia than EBN group. In this way, the flora structure was effectively regulated by EBN, SCP and SA.

Microbiota identified at the family level covered more than 92% of the total, therefore the analysis at the family level appeared quite important. Dominant families in CON group were Muribaculaceae (24.03%), Akkermansiaceae (21.17%), and Lachnospiraceae (11.34%). Compared with CON group, the abundance of Akkermansiaceae in LPS group decreased dramatically to 0.36% ($P < 0.000\ 1$), Prevotellaceae decreased significantly ($P < 0.05$) as well. In contrast, Saccharimonadaceae, Streptococcaceae and Enterococcaceae (it's in the bar of "other", the same as not shown in the figure below) increased significantly ($P < 0.05$), Desulfovibrionaceae and Deferribacteraceae rose as well ($P < 0.05$). In terms of EBN group, Lactobacillaceae and Akkermansiaceaea abundance rose, meanwhile Muribaculaceae and Aerococcaceae increased significantly ($P < 0.05$) (Fig. 11F). By contrast, Saccharimonadaceae, Desulfovibrionaceae, Deferribacteraceae and Marinifilaceae descended ($P < 0.05$). Similarly, the abundance of Muribaculaceae and Aerococcaceae increased in SCP group ($P < 0.05$). In SA group, except for rise in Muribaculaceae and reduce in Saccharimonadaceae, Prevotellaceae increased significantly ($P < 0.05$), Streptococcaceae and Enterococcaceae decreased ($P < 0.05$).

It was generally found microbiota identified at the genus level decreased significantly, and the unidentified genera in 5 groups

Table 3
α-Diversity index of gut microbiota communities ($n = 7$).

Group	Sobs index	Chao1 index	ACE index	Pielou's evenness	Shannon index	Simpson index
CON	692.00 ± 52.47	816.17 ± 51.95	815.11 ± 48.66	0.58 ± 0.07	5.52 ± 0.66	0.91 ± 0.06
LPS	694.67 ± 68.48	816.57 ± 58.85	821.59 ± 58.87	0.65 ± 0.04$^{\#}$	6.09 ± 0.37	0.96 ± 0.02$^{\#}$
EBN	645.57 ± 65.42	757.20 ± 56.27	761.77 ± 50.67	0.60 ± 0.05	5.58 ± 0.53	0.94 ± 0.02
SCP	667.80 ± 57.83	773.47 ± 57.86	773.74 ± 58.80	0.63 ± 0.03	5.94 ± 0.32	0.96 ± 0.01
SA	639.83 ± 26.63	751.76 ± 53.72	743.17 ± 39.25	0.64 ± 0.04	5.95 ± 0.37	0.96 ± 0.02

Note: $^{\#}P < 0.05$ *vs*. CON group.

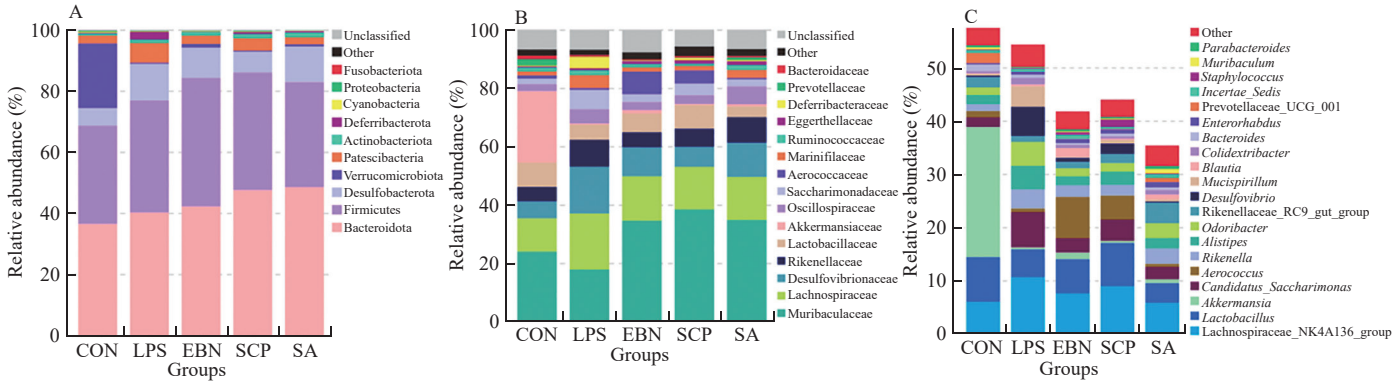

Fig. 10 Gut microbiota distribution at (A) the phylum (top 10), (B) family (top 15) and (C) genus (top 20) level. $n = 5–7$.

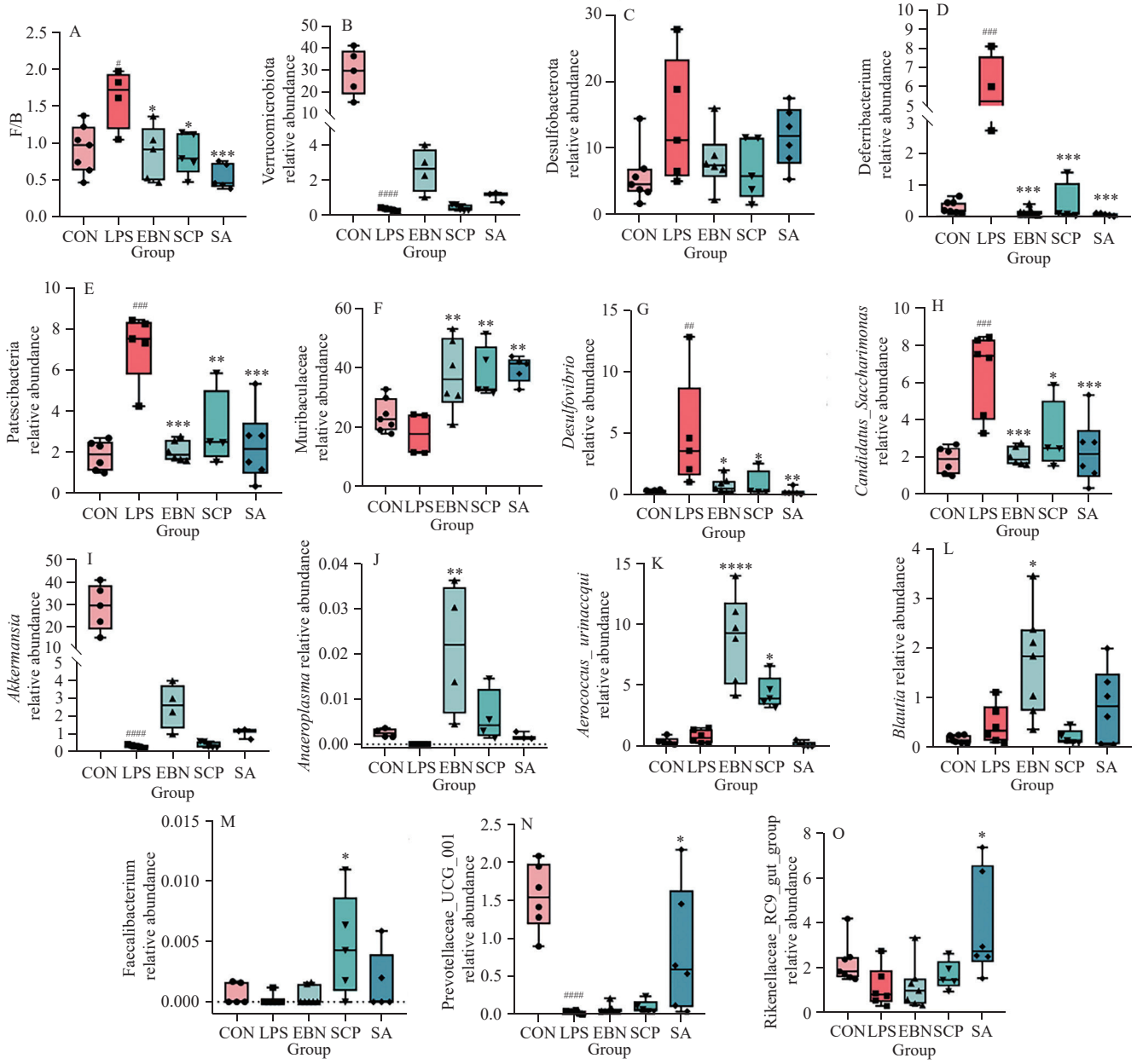

Fig. 11 Gut microbiota differences between CON, LPS, EBN, SCP and SA mice. n = 5–7. (A) F/B ratio. (B-E) Relative abundance of dominant phyla. (F) Relative abundance of Muribaculaceae at family level. (G-O) Relative abundance of dominant genera. $^{\#}P < 0.05$, $^{\#\#\#}P < 0.001$, $^{\#\#\#\#}P < 0.000\ 1$ *vs*. CON group, $^{*}P < 0.05$, $^{**}P < 0.01$, $^{***}P < 0.001$, $^{****}P < 0.000\ 1$ *vs*. LPS group.

accounted for 42.80%–64.64% of the total. Based on the results of bacteria successfully annotated, top 3 bacteria in CON group were *Akkermansia* (21.17%), *Lactobacillus* (8.09%) and Lachnospiraceae_NK4A136_group (5.95%). In the LPS mice, the abundance of *Akkermansia* in the colon decreased sharply ($P < 0.000\ 1$), Prevotellaceae_UCG_001, *Alloprevotella*, *Muribaculum*, *Dubosiella* significantly decreased as well ($P < 0.05$). *Desulfovibrio* ($P < 0.01$) and *Candidatus_Saccharimonas* ($P < 0.001$) increased significantly (Figs. 11G–H). Those indicated gut flora of LPS mice had been disturbed at the genus level. As for EBN group, the abundance of *Aerococcus* and *Blautia* increased significantly ($P < 0.05$, 0.000 1), while the abundance of *Candidatus_Saccharimonas*, *Roseburia*, *Eubacterium_xylanophilum*_group, *Eubacterium_siraeum*_group and *Lactococcus* decreased significantly ($P < 0.05$) (Figs. 11G-H and K-L). In SCP mice, *Aerococcus* and *Muribaculum* increased significantly ($P < 0.05$), while *Roseburia*, *Eubacterium_xylanophilum*_group, *Eubacterium_siraeum*_group, *Lactococcus*, *Ruminococcus* and *Bilophila* decreased significantly ($P < 0.05$) (Fig. 11K). Rikenellaceae_RC9_gut_group, Prevotellaceae_UCG_001 and *Muribaculum* in SA increased significantly ($P < 0.05$), while *Candidatus_Saccharimonas*, *Alistipes*, *Desulfovibrio*, *Enterococcus*, *Turicibacter* and *Lactococcus* decreased significantly ($P < 0.05$) (Figs. 11H and O). From the viewpoint at genus level, intervention effects between EBN and SCP on gut microbiota appeared more similar than those of SA and EBN, which also could be seen Venn diagram at OUT level (Fig. 9D).

Linear discriminant analysis (LDA) effect size (LEfSe) was used to find out the characteristic strain (biomarkers) in LPS, EBN, SCP and SA

mice (Fig. 12). As shown in Table 4, based on the LDA score higher than 2.5, *Desulfovibrio* and *Candidatus_Saccharimonas* were highly enriched in the microflora of LPS mice. When the CON group was compared to the LPS group, *Akkermansia* and *Anaeroplasma* were highly enriched in the healthy mice (LDA > 4) (Figs. 11I, J). *Aerococcus*, *Blautia*, *Asticcacaulis* and *Anaeroplasma* were enriched in EBN group (LDA > 2.8). In contrast with EBN, *Candidatus_Saccharimonas* and *Desulfovibrio* were significantly enriched in LPS model mice (LDA > 4.2). It was found that *Aerococcus* (LDA = 4.25) was significantly enriched, and *Muribaculum*, *Faecalibacterium* and *Anaeroplasma* (LDA > 2.6) were enriched in SCP mice (Fig. 11M). An opportunistic pathogen, *Bilophila* (LDA = 2.72) was found enriched in LPS. In SA group, Rikenellaceae_RC9_gut_group was

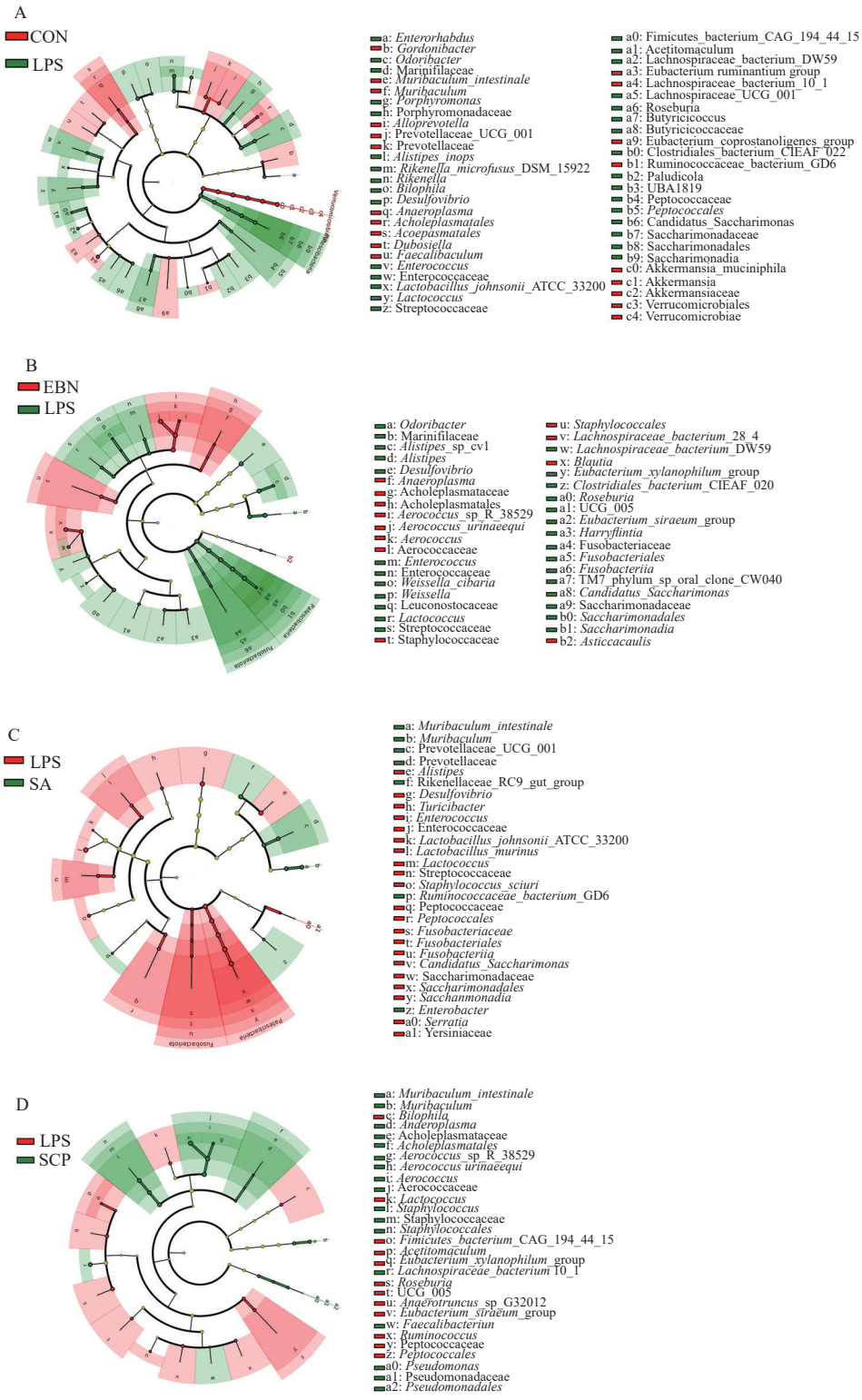

Fig. 12 LEfSe analysis for (A) CON *vs*. LPS groups, (B) EBN *vs.* LPS groups, (C) SCP *vs.* LPS groups, (D) SA *vs.* LPS groups. Only the taxa with LDA > 2.5 are shown.

firstly highly enriched (LDA = 4.14), while Prevotellaceae_UCG_001, *Muribaculum* were enriched (LDA > 3.27). Similar to EBN, *Candidatus_Saccharimonas* and *Desulfovibrio* in LPS were significantly enriched (LDA > 4).

Table 4
Genus taxon enriched by LEfSe analysis.

Comparition	Genus	Enriched group	LDA score
LPS *vs*. CON	*Desulfovibrio*	LPS	4.35
	Candidatus_Saccharimonas	LPS	4.30
	Akkermansia	CON	5.03
	Anaeroplasma	CON	4.12
EBN *vs*. LPS	*Aerococcus*	EBN	4.56
	Blautia	EBN	3.78
	Asticcacaulis	EBN	3.33
	Anaeroplasma	EBN	2.83
SCP *vs*. LPS	*Candidatus_Saccharimonas*	LPS	4.31
	Desulfovibrio	LPS	4.20
	Aerococcus	SCP	4.25
	Muribaculum	SCP	2.86
	Faecalibacterium	SCP	2.75
	Anaeroplasma	SCP	2.60
SA *vs*. LPS	*Roseburia*	LPS	3.18
	Bilophila	LPS	2.72
	Rikenellaceae_RC9_gut_group	SA	4.14
	Prevotellaceae_UCG_001	SA	3.60
	Muribaculum	SA	3.58
	Candidatus_Saccharimonas	LPS	4.29
	Desulfovibrio	LPS	4.26

In summary, *Desulfovibrio* (Desulfobacterota, Desulfovibrionaceae) and *Candidatus_Saccharimonas* (Deferribacterium, Deferribacteraceae) can be used as indicators of LPS-treated mice with inflammation, and the decreased abundance of *Akkermansia* (Verrucomicrobia, Akkermansiaceae) was also a characteristic in LPS-induced mice. On the other hand, the indicator strains of EBN group were *Aerococcus*, *Blautia*, and *Anaeroplasma*, and for SCP were *Aerococcus*, *Muribaculum*, *Faecalibacterium* and *Anaeroplasma*, and for SA were Rikenellaceae_RC9_gut_group, Prevotellaceae_UCG_001 and *Muribaculum*.

3.7 Correlation analysis between gut microbiota and host's metabolism

The function of gut microbial community in different groups of mice was predicted by PICRUSt2, so as to find out possible ways where microflora participated in to maintain host's metabolic homeostasis. Compared with CON group, the biosynthesis of tetracycline in LPS group was significantly upregulated ($P < 0.05$), while steroid biosynthesis and carotenoid biosynthesis significantly decreased ($P < 0.05$). The function of carotenoid biosynthesis was up-regulated in SCP and EBN microflora ($P < 0.05$), and steroid biosynthesis was also up-regulated by SCP ($P < 0.05$). However, what was different from EBN and SCP group was that the biosynthesis of tetracycline was down-regulated and the degradation of caprolactam was up-regulated in SA group ($P < 0.05$) (Figs. 13A-D).

The Pearson correlation analysis between differential metabolites and microflora was conducted to provide clues for the potential interaction between host metabolism and microbiome (Fig. 13E). In terms of bile acid metabolism, the top three genus taxon with high correlation ($R > 0.5$) with bile acid metabolites were *Eubacterium_xylanophilum*_group, *Muribaculum* and Rikenellaceae_RC9_gut_group. As for candidate genus taxon, it was found that *Akkermansia* and Prevotellaceae_UCG_001 were correlated with the changes of multiple differential metabolic pathways, and their effects were consistent. Specifically, *Akkermansia* and Prevotellaceae_UCG_001 was positively correlated with fumaric acid, succinic acid, malic acid, oxoglutaric acid ($P < 0.01$), positively correlated with *L*-acetylcarnitine, *L*-palmitoylcarnitine, oleoylcarnitine, arachidonyl carnitine, FA 18:5+2O, 18*R*-HEPE, 11,12-epoxyeicosatrienoic acid, acetylglycine ($P < 0.001$), and also with indole and *L*-tryptophan ($P < 0.000\ 1$). TCA cycle and fatty acid oxidative metabolism was involved in energy metabolism and balance, which suggested that *Akkermansia* and Prevotellaceae UCG_001 might be positively correlated with host energy metabolism and plasma tryptophan and indole levels. By contrast, *Candidatus_Saccharimonas* and *Desulfovibrio* were negatively correlated with energy metabolism, but positively correlated with indole derivatives, such as 3-indoleacrylic acid.

4. Discussion

Previous studies showed that the supplement of EBN was not only beneficial to brain development and intelligence enhancement of offspring[12-13], but also had a protective effect on brain from oxidative and inflammatory damage[10,31]. Therefore, in this study, the potential functional component of EBN, SCP, was extracted and enriched, and its prophylactic effects on neuroinflammation were evaluated in LPS-induced mice. In addition, the difference in physiological activity and regulation in gut microbiota of different forms of SA, including EBN glycoprotein, SCP glycopeptide and free SA was compared.

First of all, the association between excessive inflammation in the brain and adverse effects on learning and memory ability and depression had been established. Elevated biomarkers of systemic and cerebral inflammation were found in patients with mild cognitive impairment and AD[32-33]. The deterioration of inflammatory response was a persistent feature of the pathological progression of major depressive disorder. Similarly, significant increase in inflammatory biomarkers were observed in the brain of patients with depression[34]. SA supplements, represented by SCP, could significantly alleviate the decline of learning and memory, depression-like behavior induced by LPS. At the level of biochemical mechanism, it was found that SCP inhibited the increase of IL-1β, IL-6, TNF-α levels in hippocampus and cortex of LPS mice, and inhibited the activation of microglia and astrogliosis. The activation of microglia, main effector in the brain immune system, would cause neuronal damage and dysfunction under uncontrolled or chronic neuroinflammation as the brain lost its monitoring[35]. Most studies pointed out the destructive effect of activated microglia (M1 phenotype) and released molecules, including pro-inflammatory cytokine profile, expression of inducible nitric oxide synthase, CD86 and playing a neurotoxic role[3]. Astrocytes played an essential role in the innate immune response of the central nervous system, and there were inflammation-related molecular and functional characteristics in peripheral-induced

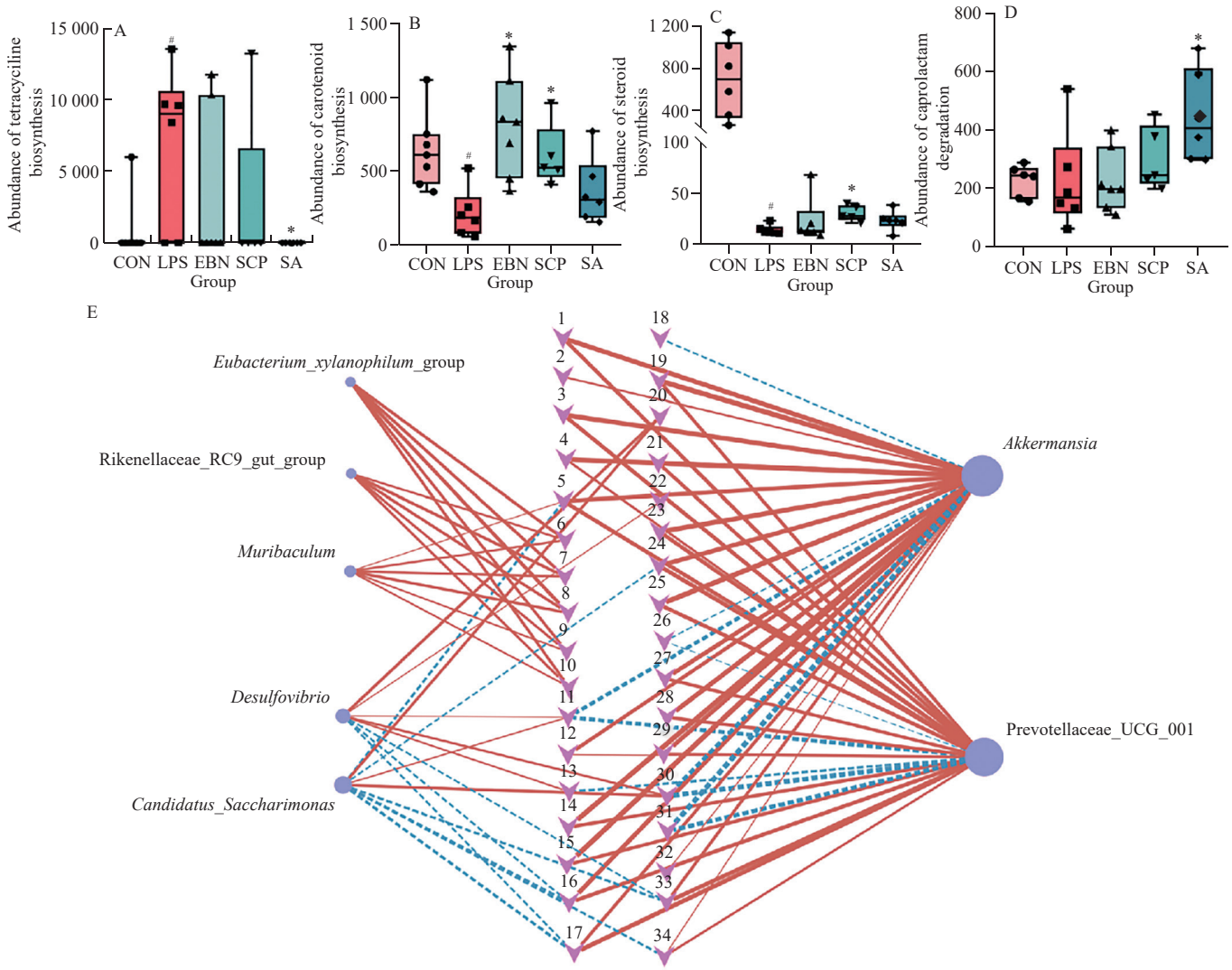

Fig. 13 (A-D) The abundance of microbiota functions predicted by PICRUSt2. n = 5–7. (E) Network of metabolites and candidate genus taxon. Circles represent genus taxon, and triangles represent metabolites. The size of circle indicates the number of associations between elements. The solid line indicates positive correlation and the dotted line indicates negative correlation; the thickness of the line indicates the R value, and thicker line indicates greater absolute value of R. 1, fumaric acid; 2, succinic acid; 3, malic acid; 4, oxoglutaric acid; 5, 3-hydroxybutyric acid; 6, deoxycholic acid; 7, 3-dehydrocholic acid; 8, cholic acid; 9, taurochenodesoxycholic acid; 10, taurocholic acid; 11, orotic acid; 12, 5-thymidylic acid; 13, gentisic acid; 14, xanthosine; 15, hypoxanthine; 16, *L*-acetylcarnitine; 17, 5-methylcytosine; 18, ascorbic acid; 19, indole; 20, 3-indoleacrylic acid; 21, *L*-tryptophan; 22, IPA; 23, *L*-palmitoylcarnitine; 24, oleoylcarnitine; 25, arachidonyl carnitine; 26, galactitol; 27, FA 18:5+2O; 28, 18*R*-HEPE; 29, 11,12-epoxyeicosatrienoic acid; 30, docosatrienoic acid; 31, 2-arachidonylglycerol; 32, thromboxane B2; 33, acetylglycine; 34, ketoleucine.

neuroinflammation, which affected the surrounding cells and then disease progression[36].

More evidence showed that peripheral inflammation triggered the immune response of the central nervous system by destroying the blood-brain barrier, recruiting immune cells and damaging cerebral vascular endothelial cells[37]. Intraperitoneal injection of inflammatory factors in mice, TNF-α and IL-1β for example, could dramatically activate inflammation in multiple brain regions[38]. Peripheral inflammation which was confirmed to induce and promote the pathological damage of the central nervous system, had been caught attention by a number of researchers[39]. The activation of serum and brain cytokine signaling in response to the peripheral or central administration of LPS was repeatedly demonstrated to mediate LPS-induced sickness behavior[40]. The method of intraperitoneal injection owned obvious advantages of shorter recovery time, less harm to animals and higher success rate and stability, so it is widely used in the establishment of neuroinflammation model[3,25,41]. LPS was a component of the cell wall of Gram-negative bacteria, a common biological factor that caused inflammation. After entering the blood, LPS was bound to CD14 receptor anchored on the membrane of Mon/macrophages and Neu in the form of LPS-LBP (LPS binding protein) complex. Subsequently, the trisomy complex interacted with Toll-like receptor 4 and its related factor MD22 to transmit signals across the membrane, triggered the subsequent intracellular signal transduction, including activating the nuclear factor kappa-B (NF-κB) signal pathway and promoting the transcription and expression of subsequent inflammatory cytokines[42]. Leukocytes were a large group of immune cells, divided into many subtypes, including Lym, Neu, Eos, Bas, Mon and macrophages. They all participated in the immune defense

response in different ways and secreted cytokines. EBN, SCP and SA were found to effectively inhibit the increase of total WBCs in blood and pro-inflammatory cytokines in serum. Moreover, the changes of Neu and Mon, with Lym no significant difference, suggested that SCP alleviated the activated nonspecific immunity by LPS infection[43]. In summary, EBN, SCP and SA was shown to exert anti-inflammatory effects, whereas their mechanism for metabolic pathway and gut microbiota differed.

Metabolomics became a popular and useful tool to evaluate the biochemical effects as metabolite information was systemically provided and metabolic pathway therefore could be visualized. Energy metabolism in LPS mice was found to decrease[44], as also evidenced by the down-regulation in malic acid, fumaric acid, succinic acid and oxoglutaric acid in our research. However, SCP could up-regulate energy metabolism as plasma malic acid, fumaric acid and succinic acid was observed a significant increase, and fumaric acid significantly increased in SA group.

An increasing number of evidence pointed to the relationship between bile acid metabolism and brain function. Defects in presence and clearance of bile acids led to many neurophenotypes, and changes in bacterial-associated bile acid levels, deoxycholic acid for instance, had been observed in human and mouse models of PD[45] as well as AD[46]. In this study, the composition of circulating bile acid pool in neuroinflammatory mice induced by LPS changed significantly, where taurine-bound cholic acid and deoxycholic acid increased significantly. It was also observed in intestinal *HIF-2α* knockout mice, and the imbalance of *Bacteroides vulgatus* and *Ruminococcus torques* led to the changes of bile acid spectrum and fat thermogenesis contributing to the weight loss of mice[47]. SCP down-regulated taurocholic acid, taurochenodesoxycholic acid and deoxycholic acid, exerting prophylactic effects on LPS-treated mice possibly through regulating bile acid metabolism. Signaling molecules alteration of bile acids' solubility and forms led to changes inbound to cellular receptors in the brain and gut, thus directly and indirectly affecting neuronal activity in multiple brain regions or the vagus nerves[48]. In fact, microbiota got closely involved in the uncoupling and biotransformation of bile acids. The function prediction by PICRUSt2 revealed that gut microbial community of SCP up-regulated steroid biosynthesis. Since bile acids and their derivatives belonged to important steroids, it was suggested again that the microbiome of SCP mice may participate in affecting the metabolism of bile acids in the host. Through the Pearson correlation analysis between bile acid derivatives and microbiota, *Eubacterium_xylanophilum_*group, *Muribaculum* and Rikenellaceae_RC9_gut_group were screened. Liu et al.[49] also reported a strong correlation between *Eubacterium_xylanophilum_*group, *Muribaculum* and most of bile acids. In this study, *Muribaculum* was highly enriched in SA group, and Rikenellaceae_RC9_gut_group was also one of the specific genera in SA mice. As primary and secondary bile acid levels detected in this study displayed an opposite trend in SA mice from that in SCP, there was different pathway behind SCP and SA of bile acids metabolism where microorganisms participated.

Another metabolic pathway of concern was tryptophan and indole. Indole and tryptophan in plasma of LPS mice decreased significantly, while IPA and indole acrylic acid (fold change = 114.49) increased significantly. Tryptophan metabolic pathway, especially 5-hydroxytryptamine (5-HT) pathway, got involved in the evolution of depression. The concentrations of plasma tryptophan and 5-HT in patients with depression were significantly lower than those in normal subjects[50-51]. In patients with AD, plasma levels of tryptophan, kynurenic acid and 5-HT were lower. The down-regulation of tryptophan indicated patients were unable to carry out daily life activities effectively[52]. In the gut, 5-HT and kynurenine pathways were among the three major tryptophan metabolism pathways, where microbiota played an important role[53]. In the direct transformation of tryptophan by intestinal microorganisms into indole and its derivatives, indole acrylic acid was reported to promote intestinal epithelial barrier function and reduce inflammation[54]. Studies proved that IPA promoted the regeneration of sensory axons of mouse sciatic nerve through immune-mediated mechanism[55]. However, in this study, plasma IPA and 3-indoleacrylic acid increased significantly in LPS-treated mice. Metabolomics analysis of serum revealed that IPA was significantly increased in people with PD[56]. IPA and butyric acid in plasma also significantly increased in benzene poisoned mouse[57], which may be the response in order to alleviate intestinal barrier injury and inflammation, or the decrease of metabolic capacity of intestinal and liver cells. Therefore, the increase of indole microbiota-derived molecules in neuroinflammatory mice was speculated to be the compensatory effect. EBN, SCP and SA all down-regulated IPA and 3-indoleacrylic acid in plasma, implying improved intestinal environment or metabolic homeostasis. In addition, rats exposed to indole in the gut displayed increased anxiety-like and depressive-like behaviors and vagal neurons were activated as well[58]. It was also of interest whether SCP exerted beneficial effects via systemic-humoral pathway combined with neuronal pathway.

Evidence was mounting that conduits of communication from the gut microbiota to the brain included activation of the vagus nerves, immune-mediated signaling and transport of gut-derived metabolites from the circulation into the brain. All routes comprising the gut-brain axis were thought to be co-opted by the microbiota to impact brain activity and behavior, and signaling through any one of them may be intertwined with other routes[59]. Therefore, diversity and composition of colon microbiota was analyzed by 16S rDNA sequence. LPS-treated mice were characterized by higher abundance of *Candidatus_Saccharimonas*, *Desulfovibrio*, and Deferribacteraceae, and *Akkermansia* almost gone, reflecting the dysfunction in intestine. In addition, EBN and its potentially active components down-regulated abundance of abnormal and harmful bacteria strains. *Desulfovibrio* belonged to a small group of sulfate-reducing bacteria, characterized by the production of H_2S from sulfur-containing compounds (mucins and amino acids). H_2S was highly toxic when it was beyond the physiological range of strict control. *Desulfovibrio* clearly flourished in an inflammatory environment, and was found reduced by diets of glycomacropeptide, a bioactive 64-amino acid peptide with high degree of glycosylation[60]. Increasing abundance of Desulfobacterota and Deferribacterota was also found in the feces of mice with type 2 diabetes mellitus[61]. Meanwhile, Deferribacteraceae was positively correlated with inflammation-related gastrointestinal diseases, such as colorectal cancer, inflammatory bowel disease and Crohn's disease[62]. The relationship between the abundance of Saccharimonadaceae and the health status of host was still unclear. However, it was found that Saccharimonadaceae and Marinifilaceae increased in lupus mouse model, and it was positively correlated with the increase of serum TNF-α, IL-1β and IL-6[63]. Zhukov et al.[64] found Saccharimonadaceae became one of the top 10 families in TAAR9-KO group, which did not exist in wild-type animal microorganism. The increase of Saccharimonadaceae abundance in TAAR9-KO rats may

reflect some disturbance of colonic microbial community and dopaminergic signal.

EBN, SCP and SA up-regulated Muribaculaceae and other specific genera to consolidate the balance and health of intestine environment, and thus maintain metabolism of host. Muribaculaceae was a mucin monosaccharide foragers[65], and found abundant in all the 3 intervention groups. Cui et al.[66] reported curcumin restored Muribaculaceae, Lactobacillaceae and Lachnospiraceae abundance in PD mice induced by mouse toxicity prevention test, which was strongly correlated with tyrosine, methionine, sarcosine and creatine in serum. Shang et al.[67] and Hao et al.[68] reported Muribaculaceae to exert anti-inflammatory activity in inflammatory bowel disease mice. As EBN, SCP and SA were sia-glycoprotein, sia-polysaccharides peptide, and monosaccharide rich in mucin, dietary supplements could improve the colonization and survival of mucin (monosaccharide) bacteria in the intestinal tract, and further playing a role in regulating host metabolism. *Akkermansia* was another kind of mucin (monosaccharide) bacteria and extensively reported as next generation of probiotics[69]. Endotoxemia could damage the integrity of intestinal tract, resulting in inhibition of the growth of *Akkermansia*[70]. On the other hand, its imbalance was likely to lead to the increase of intestinal permeability and the proliferation of related harmful bacteria, further resulting in the deterioration of inflammation and dysfunction of the host. The up-regulated abundance of *Akkermansia* might be attributed to the beneficial effects of EBN consumption *in vitro* fermentation[71], consistent with the findings in this study.

Aerococcaceae had been reported closely related to human infection, including *Aerococcus urinae*, *A. sarguinicola* and *A. viridans*. However, *Aerococcus* was the only genus in EBN and SCP microflora community. This genus had a strong ability to hydrolyze hippuric acid and decompose carbohydrate, like maltose, lactose, sucrose, trehalose, *D*-mannitol and produce *β*-glucuronidase. There were few reports of clinical infection of *A. urinaeequi*, and insufficient understanding of the bacteria[72]. In the investigation of the relationship between *Aerococcus* and host health, some contradictory conclusions were found. Son et al. [73] found that the abundance of *Aerococcus* increased in healthy neurotypical children, whereas in another study was higher in autistic children[74]. In addition, some evidence suggested *Aerococcus* abundance was higher in healthy people than patients with myasthenia gravis[75] or acne[76]. Evidence was too limited to put forward the conclusion at present. However, the abundance of *Aerococcus* in EBN and SCP increased significantly, and the role of *A. urinaeequi* in mice needed to be further explored.

Prevotellaceae in SA (specifically Prevotellaaceae_UCG_001) was significantly up-regulated, which was different from the targeted flora that EBN and SCP had regulated. It was found that increasing the proportion of resistant starch could restore the abundance of Prevotellaceae in ovariectomized rats under high-fat diet and effectively improve the ability of spatial memory[77]. In depression model mice, *Morinda officinalis* oligosaccharides up-regulated the relative abundance of Prevotellaceae_UCG_001 and *Prevotella*_9, which was widely considered to be a probiotic promoting the production of short-chain fatty acids[78].

Taken together, in order to clarify how EBN, SCP and SA exerted their neuroprotective activities through the regulation of intestinal flora, it has been found that EBN, SCP and SA significantly up-regulated the potential anti-inflammatory Muribaculaceae and inhibited pro-inflammatory related *Desulfovibrio* and *Candidatus_Saccharimonas*. In addition, both EBN and SCP could significantly enrich *A. urinaeequi*, while SA could specifically enrich Prevotellaceae_UCG_001. Meanwhile the functional prediction and correlation analysis showed microbiota was highly correlated with energy metabolism, primary and secondary bile acid metabolism, and indole metabolism, further regulating the physiology and function of the central nervous system.

5. Conclusion

SCP in EBN were extracted, and its neuroprotective effects along with EBN and SA, were observed in LPS-treated mice, proved by improvements in cognition impair and depression-like behaviors. SCP exerted anti-inflammation property, as proved by regulating leukocytes in blood, especially Neu and Mon, and alleviating increase of IL-1β, TNF-α and IL-6 in serum and hippocampus. SCP up-regulated energy metabolism, promoted the recovery of primary and secondary bile acid metabolism and indole metabolism. Changes in bile acids and indole derivatives involved in metabolism by microorganisms were also found. 16S rDNA results showed EBN, SCP and SA all enriched anti-inflammatory Muribaculaceae and inhibited pro-inflammatory related *Desulfovibrio* and *Candidatus_Saccharimonas*. Meanwhile, EBN, SCP and SA on microflora was targeted in different strains, associated with the difference in the form of SA. Gut microflora responding to SCP may specifically regulated sterol biosynthesis. Moreover, *Akkermansia* and Prevotellaceae_UCG_001 were significantly and positively correlated with host energy metabolism and plasma tryptophan and indole levels. SCP would become a potential functional food for anti-inflammation and cognitive protection. The changes of metabolic pathways and related microflora found based on high-throughput omics technology supported the protective effect of SCP on LPS-induced neuroinflammatory mice through the gut-brain axis. However, specific microflora and microorganisms-derived metabolites needed to be further verified. In addition, the characterization of SCP and its protective effects on other important organs, spleen and lung for instance, deserved to be explored in the future.

Conflict of interest

The authors declare no conflict of interest.

Acknowledgements

The project was funded by Central Nervous System Product Research and Development Key Laboratory of Sichuan Province (230048-01SZ).

Appendix A. Supplementary information

Supplementary data associated with this article can be found, in the online version, at http://doi.org/10.26599/FSHW.2024.9250289.

References

[1] D.M. Wilson, M.R. Cookson, L. van Den Bosch, et al., Hallmarks of neurodegenerative diseases, Cell 186 (2023) 693-714. https://doi.org/10.1016/j.cell.2022.12.032.

[2] W. Zhang, D. Xiao, Q. Mao, et al., Role of neuroinflammation in neurodegeneration development, Sig. Transduct. Target. Ther. 8 (2023) 267. https://doi.org/10.1038/s41392-023-01486-5.

[3] M.N. Catorce, G. Gevorkian, LPS-induced murine neuroinflammation model: main features and suitability for pre-clinical assessment of nutraceuticals, Curr. Neuropharmacol. 14 (2016) 155-164. https://doi.org/10.2174/1570159X14666151204122017.

[4] H. Bian, G. Wang, J. Huang, et al., Dihydrolipoic acid protects against lipopolysaccharide-induced behavioral deficits and neuroinflammation via regulation of Nrf2/HO-1/NLRP3 signaling in rat, J. Neuroinflammation 17 (2020) 166. https://doi.org/10.1186/s12974-020-01836-y.

[5] M.G. Fronza, R. Baldinotti, J. Fetter, et al., Beneficial effects of QTC-4-MeOBnE in an LPS-induced mouse model of depression and cognitive impairments: the role of blood-brain barrier permeability, NF-κB signaling, and microglial activation, Brain Behav. Immun. 99 (2022) 177-191. https://doi.org/10.1016/j.bbi.2021.10.002.

[6] V.E. Bianchi, P.F. Herrera, R. Laura, Effect of nutrition on neurodegenerative diseases. A systematic review, Nutr. Neurosci. 24 (2021) 810-834. https://doi.org/10.1080/1028415X.2019.1681088.

[7] Y. Dai, J. Cao, Y. Wang, et al., A comprehensive review of edible bird's nest, Food Res. Int. 140 (2021) 109875. https://doi.org/10.1016/j.foodres.2020.109875.

[8] M.Y. Yew, R.Y. Koh, S.M. Chye, et al., Edible bird's nest ameliorates oxidative stress-induced apoptosis in SH-SY5Y human neuroblastoma cells, BMC Complement. Altern. Med. 14 (2014) 391. https://doi.org/10.1186/1472-6882-14-391.

[9] Z. Hou, M.U. Imam, M. Ismail, et al., Lactoferrin and ovotransferrin contribute toward antioxidative effects of edible bird's nest against hydrogen peroxide-induced oxidative stress in human SH-SY5Y cells, Biosci. Biotechnol. Biochem. 79 (2015) 1570-1578. https://doi.org/10.1080/09168451.2015.1050989.

[10] R. Ismaeil, A.B.A. Affandi, C.K. Hui, et al., Neuroprotective effect of edible bird's nest on chronic cerebral hypoperfusion induced neurodegeneration in rats, Clin. Neurophysiol. 132 (2021) e121-e122. https://doi.org/10.1016/j.clinph.2021.02.299.

[11] M.Y. Yew, R.Y. Koh, S.M. Chye, et al., Edible bird's nest improves motor behavior and protects dopaminergic neuron against oxidative and nitrosative stress in Parkinson's disease mouse model, J. Funct. Foods 48 (2018) 576-585. https://doi.org/10.1016/j.jff.2018.07.058.

[12] Y. Xie, H. Zeng, Z. Huang, et al., Effect of maternal administration of edible bird's nest on the learning and memory abilities of suckling offspring in mice, Neural Plast. 2018 (2018) 1-13. https://doi.org/10.1155/2018/7697261.

[13] H. Zhu, Y. Li, X. Lin, et al., Maternal edible bird's nest diet improves learning and memory function of offspring rats via the ERK-CREB-BDNF pathway, J. Funct. Foods 108 (2023) 105757. https://doi.org/10.1016/j.jff.2023.105757.

[14] O. Mahaq, M.A.P. Rameli, M.J. Edward, et al., The effects of dietary edible bird nest supplementation on learning and memory functions of multigenerational mice, Brain Behav. 10 (2020) e01817. https://doi.org/10.1002/brb3.1817.

[15] Y. Fan, Y. Fan, K. Liu, et al., Edible bird's nest ameliorates dextran sulfate sodium-induced ulcerative colitis in C57BL/6J mice by restoring the Th17/Treg cell balance, Front. Pharmacol. 12 (2021) 632602. https://doi.org/10.3389/fphar.2021.632602.

[16] Q.W.S. Lai, Q. Fan, B.Z. Zheng, et al., Edible bird's nest, an Asian health food supplement, possesses anti-inflammatory responses in restoring the symptoms of atopic dermatitis: an analysis of signaling cascades, Front. Pharmacol. 13 (2022) 941413. https://doi.org/10.3389/fphar.2022.941413.

[17] T.H. Lee, W.A. Wani, C.H. Lee, et al., Edible bird's nest: the functional values of the prized animal-based bioproduct from Southeast Asia: a review, Front. Pharmacol. 12 (2021) 626233. https://doi.org/10.3389/fphar.2021.626233.

[18] C. Tung, J. Pan, H. Chang, et al., Authentic determination of bird's nests by saccharides profile, J. Food Drug Anal. 16 (2008) 86-91.

[19] N.A. Daud, S.R. Sarbini, A.S. Babji, et al., Characterization of edible swiftlet's nest as a prebiotic ingredient using a simulated colon model, Ann. Microbiol. 69 (2019) 1235-1246. https://doi.org/10.1007/s13213-019-01507-1.

[20] N. Daud, S. Mohamad Yusop, A.S. Babji, et al., Edible bird's nest: physicochemical properties, production, and application of bioactive extracts and glycopeptides, Food Rev. Int. 37 (2021) 177-196. https://doi.org/10.1080/87559129.2019.1696359.

[21] X. Wang, Q. Fan, J. Lian, et al., Study on *in vitro* digestion characteristics of bird's nest, J. Food Sci. Biotechnol. 40 (2021) 70-77.

[22] Y. You, Z. Li, C. Xue, et al., The effects of Maillard reaction on glycoproteinglycosylation in edible bird's nest and simulated gastrointestinal digestion *in vitro*, J. Chin. Inst. Food Sci. Technol. 14 (2014) 11-16.

[23] X. Xian, Y. Hou, J. Lin, et al., Study on degradation of protein of edible birds' nest (*Aerodramus*) *in vitro*, J. Chin. Med. Mater. 33 (2010) 1760-1763.

[24] T. Tan, S.L. Mun, J.L. Lee, et al., Bioactive sialylated-mucin (SiaMuc) glycopeptide produced from enzymatic hydrolysis of edible swiftlet's nest (ESN): degree of hydrolysis, nutritional bioavailability, and physicochemical characteristics, Int. J. Food Prop. 25 (2022) 252-277. https://doi.org/10.1080/10942912.2022.2029482.

[25] J. Zhao, W. Bi, S. Xiao, et al., Neuroinflammation induced by lipopolysaccharide causes cognitive impairment in mice, Sci. Rep. 9 (2019) 5790. https://doi.org/10.1038/s41598-019-42286-8.

[26] H. Luo, J. Hu, Y. Wang, et al., *In vivo* and *in vitro* neuroprotective effects of *Panax ginseng* glycoproteins, Int. J. Biol. Macromol. 113 (2018) 607-615. https://doi.org/10.1016/j.ijbiomac.2018.02.015.

[27] Z. Xie, H. Lu, S. Yang, et al., Salidroside attenuates cognitive dysfunction in senescence-accelerated mouse prone 8 (SAMP8) mice and modulates inflammation of the gut-brain axis, Front. Pharmacol. 11 (2020) 568423. https://doi.org/10.3389/fphar.2020.568423.

[28] X.R. Cheng, L.J. Guan, M.N. Muskat, et al., Effects of Ejiao peptide-iron chelates on intestinal inflammation and gut microbiota in iron deficiency anemic mice, Food Funct. 12 (2021) 10887-10902. https://doi.org/10.1039/D1FO01802G.

[29] X.R. Cheng, Y.Y. Chen, C.C. Cao, et al., Ejiao peptide-iron chelates regulate the metabolism of iron deficiency anemia mice and improve the bioavailability of iron, Food Biosci. 54 (2023) 102835. https://doi.org/10.1016/j.fbio.2023.102835.

[30] H. Tan, S.J. Lim, A.S. Babji, et al., Enzymatic hydrolysis: sialylated mucin (SiaMuc) glycoprotein of edible swiftlet's nest (ESN) and its molecular weight distribution as bioactive ESN SiaMuc-glycopeptide hydrolysate, Int. J. Biol. Macromol. 175 (2021) 422-431. https://doi.org/10.1016/j.ijbiomac.2021.02.007.

[31] S. Careena, D. Sani, S.N. Tan, et al., Effect of edible bird's nest extract on lipopolysaccharide-induced impairment of learning and memory in Wistar rats, J. Evid.-Based Complement. Altern. Med. 2018 (2018) 9318789. https://doi.org/10.1155/2018/9318789.

[32] S. Janelidze, N. Mattsson, E. Stomrud, et al., CSF biomarkers of neuroinflammation and cerebrovascular dysfunction in early Alzheimer disease, Neurology 91 (2018) e867-e877. https://doi.org/10.1212/WNL.0000000000006082.

[33] A.R. Morgan, S. Touchard, C. Leckey, et al., Inflammatory biomarkers in Alzheimer's disease plasma, Alzheimer's Dement. 15 (2019) 776-787. https://doi.org/10.1016/j.jalz.2019.03.007.

[34] E. Setiawan, A.A. Wilson, R. Mizrahi, et al., Role of translocator protein density, a marker of neuroinflammation, in the brain during major depressive episodes, JAMA Psychiat. 72 (2015) 268-275. https://doi.org/10.1001/jamapsychiatry.2014.2427.

[35] A.M. Casano, F. Peri, Microglia: multitasking specialists of the brain, Dev. Cell 32 (2015) 469-477. https://doi.org/10.1016/j.devcel.2015.01.018.

[36] B. Diaz-Castro, A.M. Bernstein, G. Coppola, et al., Molecular and functional properties of cortical astrocytes during peripherally induced neuroinflammation, Cell Rep. 36 (2021) 109508. https://doi.org/10.1016/j.celrep.2021.109508.

[37] X. Huang, J. Chang, Research progress of the effect and mechanism of peripheral inflammation on blood-brain barrier function, Cyborg. Bionic. Syst. 33 (2021) 7-14.

[38] F. Jagot, R. Gaston-Breton, A.J. Choi, et al., The parabrachial nucleus elicits a vigorous corticosterone feedback response to the pro-inflammatory cytokine IL-1β, Neuron 111 (2023) 2367-2382.e6. https://doi.org/10.1016/j.neuron.2023.05.009.

[39] Y. Li, C. Zou, C. Chen, et al., Myeloid-derived MIF drives RIPK1-mediated cerebromicrovascular endothelial cell death to exacerbate ischemic brain injury, Proc. Natl. Acad. Sci. 120 (2023) e2219091120. https://doi.org/10.1073/pnas.2219091120.

[40] R. Dantzer, J.C. O'Connor, G.G. Freund, et al., From inflammation to sickness and depression: when the immune system subjugates the brain, Nat. Rev. Neurosci. 9 (2010) 46-56.

[41] A.F.K. Vizuete, F. Fróes, M. Seady, et al., Early effects of LPS-induced neuroinflammation on the rat hippocampal glycolytic pathway, J. Neuroinflammation 19 (2022) 255. https://doi.org/10.1186/s12974-022-02612-w.

[42] Y. Wang, Post-translational modifications in regulation of lipopolysaccharide-activated signal transduction pathway, Chin. J. Biochem. Mol. Biol. 24 (2008) 505-511.

[43] H. Wang, Y. Yang, X. Zhang, et al., Liensinine attenuates inflammation and oxidative stress in spleen tissue in an LPS-induced mouse sepsis model, J. Zhejiang Univ. Sci. B 24 (2023) 185-190. https://doi.org/10.1631/jzus.B2200340.

[44] Y. Peng, Z. Shi, S.K. Satyanarayanan, et al., Fish oil alleviates LPS-induced inflammation and depressive-like behavior in mice via restoration of metabolic impairments, Brain Behav. Immun. 90 (2020) 393-402. https://doi.org/10.1016/j.bbi.2020.09.005.

[45] J. Hertel, A.C. Harms, A. Heinken, et al., Integrated analyses of microbiome and longitudinal metabolome data reveal microbial-host interactions on sulfur metabolism in Parkinson's disease, Cell Rep. 29 (2019) 1767-1777.e8. https://doi.org/10.1016/j.celrep.2019.10.035.

[46] K. Nho, A. Kueider-Paisley, S. MahmoudianDehkordi, et al., Alzheimer's disease neuroimaging initiative and the Alzheimer disease metabolomics consortium, altered bile acid profile in mild cognitive impairment and Alzheimer's disease: relationship to neuroimaging and CSF biomarkers, Alzheimers Dement. 15 (2019) 232-244. https://doi.org/10.1016/j.jalz.2018.08.012.

[47] Q. Wu, X. Liang, K. Wang, et al., Intestinal hypoxia-inducible factor 2α regulates lactate levels to shape the gut microbiome and alter thermogenesis, Cell Metab. 33 (2021) 1988-2003.e7. https://doi.org/10.1016/j.cmet.2021.07.007.

[48] K.L. Mertens, A. Kalsbeek, M.R. Soeters, et al., Bile acid signaling pathways from the enterohepatic circulation to the central nervous system, Front. Neurosci. 11 (2017) 617. https://doi.org/10.3389/fnins.2017.00617.

[49] X. Liu, Y. Zhang, W. Li, et al., Fucoidan ameliorated dextran sulfate sodium-induced ulcerative colitis by modulating gut microbiota and bile acid metabolism, J. Agric. Food Chem. 70 (2022) 14864-14876. https://doi.org/10.1021/acs.jafc.2c06417.

[50] W. Marx, A.J. McGuinness, T. Rocks, et al., The kynurenine pathway in major depressive disorder, bipolar disorder, and schizophrenia: a meta-analysis of 101 studies, Mol. Psychiatry 26 (2021) 4158-4178. https://doi.org/10.1038/s41380-020-00951-9.

[51] R. Colle, P. Masson, C. Verstuyft, et al., Peripheral tryptophan, serotonin, kynurenine, and their metabolites in major depression: a case-control study, Psychiatry Clin. Neurosci. 74 (2020) 112-117. https://doi.org/10.1111/pcn.12944.

[52] C. Xue, G. Li, Q. Zheng, et al., Tryptophan metabolism in health and disease, Cell Metab. 35 (2023) 1304-1326. https://doi.org/10.1016/j.cmet.2023.06.004.

[53] A. Agus, J. Planchais, H. Sokol, Gut microbiota regulation of tryptophan metabolism in health and disease, Cell Host Microbe 23 (2018) 716-724. https://doi.org/10.1016/j.chom.2018.05.003.

[54] M. Wlodarska, C. Luo, R. Kolde, et al., Indoleacrylic acid produced by commensal peptostreptococcus species suppresses inflammation, Cell Host Microbe 22 (2017) 25-37.e6. https://doi.org/10.1016/j.chom.2017.06.007.

[55] E. Serger, L. Luengo-Gutierrez, J.S. Chadwick, et al., The gut metabolite indole-3 propionate promotes nerve regeneration and repair, Nature 607 (2022) 585-592. https://doi.org/10.1038/s41586-022-04884-x.

[56] D. Rosario, G. Bidkhori, S. Lee, et al., Systematic analysis of gut microbiome reveals the role of bacterial folate and homocysteine metabolism in Parkinson's disease, Cell Rep. 34 (2021) 108807. https://doi.org/10.1016/j.celrep.2021.108807.

[57] J. Wang, L. Han, Z. Liu, et al., Genus unclassified_Muribaculaceae and microbiota-derived butyrate and indole-3-propionic acid are involved in benzene-induced hematopoietic injury in mice, Chemosphere 313 (2023) 137499. https://doi.org/10.1016/j.chemosphere.2022.137499.

[58] M. Jaglin, M. Rhimi, C. Philippe, et al., Indole, a signaling molecule produced by the gut microbiota, negatively impacts emotional behaviors in rats, Front. Neurosci. 12 (2018) 216. https://doi.org/10.3389/fnins.2018.00216.

[59] B.D. Needham, R. Kaddurah-Daouk, S.K. Mazmanian, Gut microbial molecules in behavioural and neurodegenerative conditions, Nat. Rev. Neurosci. 21 (2020) 717-731. https://doi.org/10.1038/s41583-020-00381-0.

[60] E.A. Sawin, T.J. de Wolfe, B. Aktas, et al., Glycomacropeptide is a prebiotic that reduces *Desulfovibrio* bacteria, increases cecal short-chain fatty acids, and is anti-inflammatory in mice, Am. J. Physiol Gastr. L. 309 (2015) G590-G601. https://doi.org/10.1152/ajpgi.00211.2015.

[61] D. Lu, Y. Zhao, P. Jin, et al., Effect of mulberry leaf combined with metformin on glucose and lipid metabolism disorder, inflammation and gut microbiota dysbiosis in type 2 diabetes mellitus mice, Cent. South Pharm. 21 (2023) 2560-2569.

[62] H. Zhang, Z. Zhang, G. Song, et al., Development of an XBP1 agonist, HLJ2, as a potential therapeutic agent for ulcerative colitis, Eur. J. Pharm. Sci. 109 (2017) 56-64. https://doi.org/10.1016/j.ejps.2017.07.028.

[63] Y.F. Chen, A.H. Hsieh, L.C. Wang, et al., Fecal microbiota changes in NZB/W F1 mice after induction of lupus disease, Sci. Rep. 11 (2021) 22953. https://doi.org/10.1038/s41598-021-02422-9.

[64] I.S. Zhukov, A.N. Vaganova, R.Z. Murtazina, et al., Gut microbiota alterations in trace amine-associated receptor 9 (TAAR9) knockout rats, Biomolecules 12 (2022) 1823. https://doi.org/10.3390/biom12121823.

[65] K. Hiraishi, F. Zhao, L.H. Kurahara, et al., Lactulose modulates the structure of gut microbiota and alleviates colitis-associated tumorigenesis, Nutrients 14 (2022) 649. https://doi.org/10.3390/nu14030649.

[66] C. Cui, Y. Han, H. Li, et al., Curcumin-driven reprogramming of the gut microbiota and metabolome ameliorates motor deficits and neuroinflammation in a mouse model of Parkinson's disease, Front. Cell Infect. Microbiol. 12 (2022) 887407. https://doi.org/10.3389/fcimb.2022.887407.

[67] L. Shang, H. Liu, H. Yu, et al., Core altered microorganisms in colitis mouse model: a comprehensive time-point and fecal microbiota transplantation analysis, Antibiotics 10 (2021) 643. https://doi.org/10.3390/antibiotics10060643.

[68] H. Hao, X. Zhang, L. Tong, et al., Effect of extracellular vesicles derived from *Lactobacillus plantarum* Q7 on gut microbiota and ulcerative colitis in mice, Front. Immunol. 12 (2021) 777147. https://doi.org/10.3389/fimmu.2021.777147.

[69] C. Depommier, A. Everard, C. Druart, et al., Supplementation with *Akkermansia muciniphila* in overweight and obese human volunteers: a proof-of-concept exploratory study, Nat. Med. 25 (2019) 1096-1103. https://doi.org/10.1038/s41591-019-0495-2.

[70] Q. Yu, F. Yu, Q. Li, et al., Anthocyanin-rich butterfly pea flower extract ameliorating low-grade inflammation in a high-fat-diet and lipopolysaccharide-induced mouse model, J. Agric. Food Chem. 71 (2023) 11941-11956. https://doi.org/10.1021/acs.jafc.3c02696.

[71] J. Wu, P. Lu, H. Zhang, et al., Comparison of prebiotic activity of dietary sialoglycoprotein and *N*-acetylneuraminic acid: sialylation is a key factor, Food Biosci. 56 (2023) 103397. https://doi.org/10.1016/j.fbio.2023.103397.

[72] W. Zhou, P. Gu, H. Shen, Classification and clinical infection of Aerococcus, J. Microbiol. 41 (2021) 107-113.

[73] J.S. Son, L.J. Zheng, L.M. Rowehl, et al., Comparison of fecal microbiota in children with autism spectrum disorders and neurotypical siblings in the Simons simplex collection, PLoS ONE 10 (2015) e0137725. https://doi.org/10.1371/journal.pone.0137725.

[74] A. Tomova, K. Soltys, G. Repiska, et al., Specificity of gut microbiota in children with autism spectrum disorder in Slovakia and its correlation with astrocytes activity marker and specific behavioural patterns, Physiol. Behav. 214 (2020) 112745. https://doi.org/10.1016/j.physbeh.2019.112745.

[75] D. Qiu, Z. Xia, X. Jiao, et al., Altered gut microbiota in myasthenia gravis, Front. Microb. 9 (2018) 2627. https://doi.org/10.3389/fmicb.2018.02627.

[76] Y. Deng, H. Wang, J. Zhou, et al., Patients with acne vulgaris have a distinct gut microbiota in comparison with healthy controls, Acta Derm. Venereol. 98 (2018) 783-790. https://doi.org/10.2340/00015555-2968.

[77] S. Zhang, L. Zeng, J. Ma, et al., Gut Prevotellaceae-GABAergic septohippocampal pathway mediates spatial memory impairment in high-fat diet-fed ovariectomized mice, Neurobiol. Dis. 177 (2023) 105993. https://doi.org/10.1016/j.nbd.2023.105993.

[78] Z.W. Zhang, C.S. Gao, H. Zhang, et al., *Morinda officinalis* oligosaccharides increase serotonin in the brain and ameliorate depression via promoting 5-hydroxytryptophan production in the gut microbiota, Acta Pharm. Sin. B 12 (2022) 3298-3312. https://doi.org/10.1016/j.apsb.2022.02.032.